Relative Roles of Elevated Heating and Surface Temperature Gradients in Driving Anomalous Surface Winds over Tropical Oceans

JOHN C. H. CHIANG*

Lamont-Doherty Earth Observatory of Columbia University, Palisades, New York

STEPHEN E. ZEBIAK

Lamont-Doherty Earth Observatory of Columbia University, and International Research Institute for Climate Prediction, Palisades, New York

MARK A. CANE

Lamont-Doherty Earth Observatory of Columbia University, Palisades, New York

(Manuscript received 25 August 1999, in final form 8 July 2000)

ABSTRACT

Elevated heating by cumulus convection and sea surface temperature gradients are both thought to contribute to surface winds over tropical oceans. The relative strength and role of each mechanism is examined by imposing forcing derived from data on a linear primitive equation model with idealized parameterizations for the two forcings, and comparing the response with observed surface winds. Two test cases are studied: one related to the El Niño–Southern Oscillation, and the other related to the ''dipole'' mode in the tropical Atlantic. It is found that in both cases, elevated heating dominates the surface zonal wind response, and contributes significantly to the meridional wind response, especially in the subtropics and the South Pacific and South Atlantic convergence zone regions. Surface temperature gradients dominate the meridional wind forcing in regions near the equator with strong meridional temperature gradients.

1. Introduction

The time mean surface winds over tropical oceans obey, to a very good approximation, a three-way balance between the Coriolis, friction (parameterized to be linearly proportional to the wind), and pressure gradient terms. The linear friction coefficient is roughly constant in time, although the friction coefficient for v is two to three times larger than that for u, and both coefficients vary with latitude (Deser 1993; Li and Wang 1994; Chiang and Zebiak 2000). Hence, the question of what drives surface winds is largely a question of what influences surface pressure gradients. Two thermal influences on surface pressure are usually considered: elevated heating by cumulus convection, and sea surface temperature (SST). Each has motivated a simple dynamical framework for the origins of tropical surface winds.

The first model is attributed to Gill (1980). Noting that cumulus heating has a characteristic vertical profile, he argued that the atmospheric response to the heating projects largely to one vertical mode—the ''first baroclinic mode.'' Assuming linear dynamics, he simplified the relevant dynamical equations to a linear dissipative shallow water equation with an equivalent depth characteristic of the vertical profile of heating. He was then able to examine analytically the surface wind response to elevated heating. The second model is attributed to Lindzen and Nigam (1987, hereafter LN). They noted that observed air temperature in the boundary layer is closely correlated with SST, presumably due to turbulent mixing, and asked how this by itself (i.e., in the absence of influence above the boundary layer) influences surface pressure. Assuming a boundary layer air temperature tied to SST, an air density solely a function of temperature, and a constant geopotential at the top of the boundary layer (taken to be 700 mb), and using the hydrostatic approximation, they backed out the surface pressure and hence surface winds. A ''back-pressure'' effect—parameterized as a linear damping on the eddy

* Current affiliation: Joint Institute for the Study of the Atmosphere and Ocean, University of Washington, Seattle, Washington.

Corresponding author address: John C. H. Chiang, Joint Institute for the Study of the Atmosphere and Ocean, Box 354235, University of Washington, Seattle, WA 98195-4235.
E-mail: jchiang@atmos.washington.edu

geopotential—was required to limit the amount of convergence generated by the model winds. They justified this step physically as a cumulus uptake of mass out of the boundary layer.

These models are far from perfect, either from a theoretical point of view, or from the more practical point of view of application. The mathematical expression of both models turns out to be similar—that of a linear dissipative shallow water system (Neelin 1989)—although the physical meaning of the model coefficients, in particular the frictional dissipation, differs depending on the paradigm used. For realistic simulations using the Gill model, the dissipation timescale is on the order of 1–2 days, which is problematic since it is unclear where the dissipation originates. The LN model draws criticism for its unrealistically thick planetary boundary layer (~300 mb) and short (~30 min) damping timescale. Recently, Battisti et al. (1999) improved the LN framework by using a 1½-layer reduced gravity setup that gave more realistic model coefficients. We refer the reader to their article, and also to Wang and Li (1993), for their excellent discussions on the theoretical comparison between the two models.

Our concern is with the practical application of the Gill and LN paradigms. The basic problem is to know when each is applicable; and indeed, if they are any good at all. This applies both to construction of simple tropical circulation models, and also with interpreting surface wind from observations or model output. Neither paradigm was intended to be applicable to the entire Tropics: Gill's paradigm was intended for convectively driven near-equatorial zonally asymmetric circulation, and LN was meant to be operative only where stratocumulus and trade-cumulus boundary layers (capped by an inversion) occur. However clearly there is a degree of overlap between these two regions, not least because of the large zonal and meridional scale of atmosphere response to elevated heating. There is also the practical difficulty of limiting model domains when constructing simple models.

Both Gill and LN model simulations of anomalous surface wind, even when using ''quasi-perfect'' forcing derived from observations, tended to be poor. For example, Nigam and Shen (1993) showed that the Gill model, when forced with observed El Niño–Southern Oscillation (ENSO)-covariant outgoing longwave radiation anomalies, gave poor simulations of both zonal and meridional winds in the central and eastern Pacific. Wagner and Da Silva's (1994) simulation of tropical Atlantic surface wind anomalies associated with wet minus dry composites of Guinea rainfall using the LN model (using a 0.75-day Rayleigh damping timescale and a very short damping timescale of 4 min) was also relatively poor, although the meridional component fared better than the zonal component. Despite these shortcomings, both paradigms have been influential in conceptualizing the causes and consequences of tropical surface wind. For example, Zebiak (1982, 1986) used the Gill paradigm to model ENSO effect on surface winds. Xie and Philander (1994) assumed the Gill paradigm in their simple zonally symmetric coupled model study of the ITCZ, but then interestingly switched to the LN paradigm for later studies (e.g., Xie 1999). Hastenrath and Greischar (1993) used the LN paradigm to understand the linkage between SST and wind anomalies associated with droughts over northeast Brazil.

It seems apparent that for a more complete model of surface winds, both influences need to be taken into account. Wang and Li (1993) attempted to do this with an LN type boundary layer below a Gill-type atmosphere. To do this, they needed to make certain model assumptions about how the free atmosphere influences surface flow. However, how the elevated heating dynamically influences surface flow is really at the heart of this problem. We draw guidance and motivation to answering this problem from a recent paper by Wu et al. (1999a), who tied this question, within a linear β-plane framework, to the role of frictional and thermal dissipation (see section 2). Our study attempts to address the question of how each forcing—elevated heating, and surface temperature gradients (hereafter referred to simply as ''surface forcing'')—relates to the monthly mean anomalous surface winds in the Tropics.

Our paper proceeds as follows. To motivate our approach, we first summarize the studies of Wu et al. (1998, 1999a), paying close attention to what they say about the effect of dissipation on forced atmospheric response. We then introduce our own model for surface winds, and outline our test, which focuses on simulating two features associated with tropical climate variability: the mature ENSO phase and the tropical Atlantic ''dipole.'' The rest of the paper is then devoted to verifying and understanding our model. In particular, we simulate the June–August (JJA) climatological eddy (deviation from zonal mean) surface wind, as well as a monthly anomaly simulation from January 1979 to December 1998. Also, a sensitivity study is done to show how various components of the model affect the surface wind simulation. We end with a discussion of our results and their implications, in particular for tropical Atlantic climate variability.

2. Motivation

Wu et al. (1998, 1999a) studied the response of the atmosphere to steady, large-scale, elevated heating. They looked for analytical solutions to the three-dimensional linearized steady-state equations incorporating both Newtonian cooling and Rayleigh friction, focusing specifically on the surface wind response. In particular, they looked at the extreme cases of a Newtonian-cooling-dominated and a Rayleigh-friction-dominated regime. While the analysis involved some demanding mathematics, the physical implications are straightforward. They find that Newtonian cooling and Rayleigh friction play totally different roles in the tropical at-

mosphere. Newtonian cooling acts to homogenize the response in the vertical, and in particular a vertically uniform response is found below the heating region, extending to the surface. On the other hand, in a Rayleigh friction dominated regime, the response to elevated heating is confined to the levels of heating, and little response is felt at the surface. The addition of dissipation changes the properties of the vertical structure equation. Wu et al. offers a physically intuitive explanation for why a surface response occurs in a Newtonian-cooling-dominated regime. The cooling acts to pull the temperature anomalies below the heating region back to zero. Hence, the geopotential gradients found at the bottom of the heating region extend relatively unchanged down to the surface.

To answer the question of whether elevated heating affects surface winds in the real atmosphere, they applied an imposed heating to a dynamical core with uniform Newtonian cooling, and friction applied below the heating region to mimic a crude boundary layer. Consistent with their analysis, they found that the presence of the frictional boundary layer dramatically reduces the surface circulation that was found for the Newtonian-cooling-only case. They suggest from this study that a significant surface circulation will unlikely be driven by an elevated heat source, unless the base of the heat source is embedded well within the frictional boundary layer.

In this paper, we extend this methodology to examine the relative roles of elevated heating and surface temperature gradients in driving surface winds, but under more realistic model parameterizations and tuning. In particular, it is clear that realistic dissipation timescales are crucial. We question Wu et al.'s choice of a uniform Newtonian cooling as the only thermal dissipation mechanism, since temperature anomalies are damped much more rapidly in the boundary layer due to turbulent transfer and radiative effects of clouds and moisture, relative to the free atmosphere. Also, even if an elevated heat source cannot influence surface pressure gradients, it may be possible for winds above the boundary layer generated by elevated heating to influence surface winds through turbulent mixing (Chiang and Zebiak 2000). Finally, heating by cumulus convection is not just restricted to above the frictional boundary layer. In fact, the lifting condensation level (LCL) is generally well below the typical boundary layer top height of around 800 mb in the convectively active regions. Below the LCL, there may be diabatic cooling associated with convective downdrafts, and reevaporation of precipitation.

We propose a more concrete test of the relative roles of elevated heating and surface temperature gradients by incorporating both forcings in an idealized model setup, but with more realistic parameterizations. In particular, we use a more realistic vertical heating profile, and a flux-gradient parameterization of the planetary boundary layer (PBL). We objectively analyze the relative roles of each mechanism by deriving a consistent set of forcing and surface wind fields from observations, and comparing the model output winds from each mechanism, with the observed surface winds. We include details of the model, observational data, and experimental setup in the next section.

3. Model description

We use the dynamical core of Seager and Zebiak (1995) as the basis for our model, with R20 truncation (64 longitude by 60 latitude grid points), and 20 equispaced σ levels in the vertical. The model is linearized about a rest basic state, the basic-state temperature being a horizontally uniform but vertically varying profile, with stratification typical for the tropical atmosphere. Vertical advection of the basic-state stratification is included. As the simplest treatment for radiation, we impose uniform Newtonian relaxation on the atmosphere below $\sigma = 0.2$, with a rate r_N, back to zero perturbation temperature. Values for parameters such as r_N are chosen from a tuning procedure, which we will describe in the next section.

The model has a rigid lid, which means that the external barotropic mode is not present. The neglect of the external barotropic mode is not thought to have a significant effect: Geisler and Stevens (1982) show that the projection of an idealized convective forcing profile on the external mode is fully an order of magnitude smaller than the dominant internal mode. Also, the imposition of a rigid lid can produce spurious resonance (Lindzen et al. 1968) under forced oscillations. This is a consequence of wave reflection at the rigid boundary. The common practice to reduce such reflection is to damp the waves near the top of the model atmosphere: in our model, we linearly increase the Newtonian relaxation rate from r_N at $\sigma = 0.2$ to 2 day^{-1} at $\sigma = 0$.

For friction, we apply a vertical diffusion of momentum of the form

$$\frac{\partial \mathbf{v}(\sigma)}{\partial t} \sim c\frac{\partial}{\partial \sigma}\left(\sigma^2\frac{\partial}{\partial \sigma}\right)\mathbf{v}(\sigma) \qquad \sigma > 0.1, \tag{1}$$

where $\mathbf{v}$ is the horizontal wind vector on a σ surface. This parameterizes the effect of turbulent transfer in the boundary layer, weakening away from the surface as it should. The eddy viscosity coefficient c is a tuned parameter. The surface momentum flux condition is taken to be linearly proportional to the anomalous wind:

$$\tau = -\frac{g\rho}{p_*}C_D|\overline{U}|\mathbf{v}_{nz} \equiv -Y\mathbf{v}_{nz}. \tag{2}$$

The subscript ''nz'' indicates the lowest model layer, which is at $\sigma = 0.975$. The effective exchange coefficient Y is a tuned parameter. In addition, we found it necessary to include Rayleigh friction above the boundary layer in order to obtain realistic wind magnitudes there. This is implemented as

$$\frac{\partial \mathbf{v}}{\partial t}(\sigma) \sim -r_F(\sigma)\mathbf{v}(\sigma), \tag{3a}$$

where r_F has the functional form

$$r_F(\sigma) = R_{FMAX}0.5 \tanh[10(0.75 - \sigma) + 1]. \tag{3b}$$

This profile applies friction at a rate close to r_{FMAX} above a height of $\sigma = 0.6$, and at a rate close to zero below a height of $\sigma = 0.8$. Between $\sigma = 0.6$ and $\sigma = 0.8$, the function transitions smoothly between the two extreme values. The friction amplitude r_{FMAX} is a tunable parameter. Finally, a biharmonic diffusion with viscosity coefficient 5×10^{16} m^4 s^{-1} is applied in the horizontal at all sigma levels to damp traveling waves. We found the model to be not sensitive to the value of the viscosity coefficient, at least for $\pm 50\%$ change to the set value, so we did not include this parameter in the tuning procedure.

Elevated heating is imposed in the model. We found from experimentation that surface wind in the model is sensitive to the specification of the heating profile, a behavior consistent with the model study by Hartmann et al. (1984), and the theoretical analysis of Wu et al. (1999b). There is observational evidence showing that the vertical profile of convective heating varies from region to region, and also over time. For example, the diabatic heating profile derived from Tropical Ocean Global Atmosphere Coupled Ocean–Atmosphere Response Experiment (TOGA COARE) data (DeMott and Rutledge 1998) shows a peak diabatic heating centered on the 700–800-mb level during cruise 2 of TOGA COARE, and centered around the 500-mb level during cruise 3. Thompson et al. (1979) show West Pacific convective heating peaking around 450 mb, whereas East Atlantic heating [measured during the Global Atmospheric Research Program's Atlantic Tropical Experiment (GATE)] peaks much lower at around 700 mb.

We idealize convective heating with a half-sine curve peaking in the midtroposphere, but allow for variation in the level of the peak by adding a perturbation consisting of a full sine curve. This perturbation shifts the maximum of heating depending on the amplitude that is chosen; this amplitude constitutes another parameter to be chosen. More specifically, the profile has this functional form:

$$P(\sigma) = \frac{\pi}{2(\sigma_B - \sigma_T)}\left[\sin\left(\pi\frac{\sigma - \sigma_T}{\sigma_B - \sigma_T}\right) + \frac{b}{2}\sin\left(2\pi\frac{\sigma - \sigma_T}{\sigma_B - \sigma_T}\right)\right], \tag{4}$$

where σ_T and σ_B define the top and bottom of the heating profile, respectively, and b ranges from -1 to 1. The range ensures that the profile does not become negative anywhere. The profile outside (σ_T, σ_B) is set to zero. The heating top σ_T is fixed in our model runs, using climatological deep convective cloud-top heights as found in the International Satellite Cloud Climatology Project (ISCCP) D2 dataset (Rossow et al. 1996). Unlike σ_T that has variation in the horizontal, the heating bottom σ_B is taken to be constant in σ, and is a tunable parameter.

The boundary layer heating is parameterized simply as a relaxation of the boundary layer grid points to the specified SST anomaly:

$$\frac{\partial T}{\partial t}(\sigma) \sim -r_{BL}(T(\sigma) - \text{SSTA}) \qquad \sigma \geq \sigma_{BL}. \tag{5}$$

More accurately, the SSTA should be multiplied by a mean lapse rate to account for the fact that a well-mixed boundary layer is characterized by fixed potential temperature, and not fixed temperature. However, the correction is less than 7% at a typical PBL top height of 800 mb, so given the crudeness of the parameterization and the errors in the model input and validation data, this correction is unwarranted. The boundary layer top height σ_{BL} is uniform in σ, and is a tunable parameter. The boundary layer thermal relaxation rate r_{BL} is also a tunable parameter.

Note that we parameterize momentum and thermal PBL processes in distinctly different ways. We chose Newtonian relaxation over a fixed depth as a simple and physically intuitive way to parameterize the thermal PBL, and that furthermore this form of parameterization is consistent with the LN idea of a well-mixed thermal boundary layer. On the other hand, Rayleigh friction applied over PBL—the momentum equivalent of how we constructed the thermal PBL—is not appropriate since we know that Ekman dynamics is important for simulating the turning of the PBL winds.

We include mountains primarily for more accurate representation of the effects of topography on the large-scale flow. Specifically, there are suggestions that the Andes play a significant role in determining eastern Pacific surface winds (Battisti et al. 1999; Zebiak 1986). We were also concerned about how remotely forced winds (e.g., the possible influence of Pacific heating on Atlantic surface winds) might be modified by the presence of intervening topography. Our topography is derived from the ETOPO5 Navy database, which has topography on a 5×5 minute grid. We interpolate to R20 resolution by averaging over each gridbox. No attempt has been made to spectrally smooth the topography, since the model simulations are not sensitive to Gibbs ripples that are a feature of topography with truncated spectral representation.

The parameterizations we chose are based on the simplest representations of what we think are important for modeling surface winds, based on the experience of previous simple model studies. There are many assumptions, amongst those being: choice of a quiescent basic state (over a more realistic basic state); lack of extratropical, and land thermal, influence; simplification of radiation to simple Newtonian cooling; and linear

dynamics. Past experience suggests that more realistic basic states do not qualitatively change the nature of the solution in the Tropics. Transient eddies are thought to feature significantly in the surface momentum balance poleward of ~15° N and S (Murphree and van den Dool 1988). Land heating from neighboring continents (especially West Africa) is thought to be important for tropical Atlantic surface circulation (Li and Philander 1997). We circumvent the lack in representation of transient eddy and land effects by deriving a surface wind field that is statistically associated with the applied forcing (see next section).

The assumption of Newtonian cooling is harder to justify. Many have employed this technique, seemingly successfully, for simulating the tropical circulation (e.g., Seager and Zebiak 1995). Newtonian cooling has the advantage of easy analysis; in particular, the works by Wu et al. (1998, 1999a) give us a framework to understand the effects of linear dissipation on elevated heating responses. Finally, our use of linear dynamics is in keeping with previous diagnostics (e.g., Deser 1993) that suggest that nonlinearity is not important for the surface momentum balance over tropical oceans. However, nonlinear dynamics has been shown to be important for the tropical upper-troposphere circulation (Sardeshmukh and Hoskins 1985) and may impact the surface circulation through its effect on surface pressure, and also through vertical mixing of momentum into the boundary layer. Our model does not have the necessary physics to model this upper-level circulation, and the need for Rayleigh friction to damp the upper-level flow may be a consequence of this. However, our own experience, and results of previous simple model studies, suggests that nonlinearity in the free atmosphere is of secondary consideration as far as modeling surface winds is concerned.

While the Gill and LN models are the motivating components of our study, we are not directly testing their validity, because of the dynamical framework we use and the way we parameterize the forcing. Specifically, the inclusion of many vertical modes, and an Ekman boundary layer, go beyond that of a pure Gill model. Also, our surface-forcing parameterization assumes that horizontal temperature gradients are well mixed vertically within the PBL everywhere in the tropical oceans, which is definitely not the case in the real atmosphere. In this sense, surface forcing might be overrepresented in the model formulation. Also, by assuming a constant thermal boundary layer height over the tropical oceans, we exclude the possible significant influence of spatial variations in both mean and anomalous boundary layer height on surface-gradient-forced surface winds. We are limited in this regard by the lack of sufficiently accurate global estimates of PBL height. Finally, since our model does not resolve the PBL inversion in the basic-state vertical temperature structure in those regions where LN is assumed to be active, we cannot fully test the LN assumption that the inversion is crucial for limiting the impact of elevated heating on surface tropical flow, although we do pursue a limited sensitivity study of the impact of the imposed vertical basic state (section 7).

4. Experimental setup

a. Derivation of forcing and observed wind response

We take precipitation forcing from the Xie and Arkin (1997) monthly mean global gridded dataset, and monthly mean 975-mb winds and SST from the National Centers for Environmental Prediction–National Center for Atmospheric Research (NCEP–NCAR) reanalysis (Kalnay et al. 1996). The time period of the data is January 1979–December 1998. Since the reanalysis surface winds and SST are strongly constrained by data, our forcing fields and response are essentially independently derived.

The model determines the choice of wind level, since 975 mb is the lowest model level. The model has an Ekman layer, but not a surface layer, parameterization, so it is more appropriate to compare winds away from the surface. However, we acknowledge the problem of how well surface wind observations constrain the 975-mb flow. It depends on the quality of the reanalysis parameterization of the frictional boundary layer. The T62 NCEP global spectral model used in the data assimilation (Kanamitsu 1989) has both a surface-layer and mixed layer parameterization, with five levels in the boundary layer. The bulk aerodynamic formulas have proportionality constants that depend on local wind and static stability, and the mixed layer has a Richardson number–dependent vertical diffusion. In other words, the boundary layer parameterization is as good as can be expected of current general circulation models (GCMs). There is also error coming from interpolation onto the model grid at 975 mb. Since boundary layer flow is generally highly correlated in the vertical, we feel that estimating reanalysis data at 975 mb is qualitatively correct.

The task is to derive anomalous winds, precipitation, and SST that are convincingly associated with each other. Here we take an approach similar to that of Nigam and Shen (1993), in which they assessed the quality of surface wind simulations in a Gill model by using data to provide both the input (heating) and the target (surface winds) for the model. We take a multivariate and unlagged empirical orthogonal function (EOF) of the forcings (monthly SST and precipitation anomalies) and the response (anomalous monthly 975-mb winds), keeping the first (dominant) mode. More specifically, each forcing and wind field was first prefiltered by computing individual EOFs, and truncating to the first 40 EOFs. These first 40 EOFs were the bulk of the variance for each field (over 80%). This EOF prefiltering allowed the computation to be kept to manageable size, without compromising spatial resolution. The multivariate EOF

was then computed by combining the 40 EOF time series of each forcing and wind field in a single EOF computation. Simultaneous fields are appropriate since the bulk of the wind response to the forcings is realized on the order of a few days. As with Nigam and Shen (1993), each field is normalized by its standard deviation (over all space and time points), so that they have equal weight. The advantages of deriving forcing and response fields in this way are: (i) random errors in the data are reduced; (ii) the response is more convincingly tied to the forcing, since they share the same time series; and (iii) the dominant EOF mode is more likely to have a physical basis (i.e., we are not just modeling noise). Under our linearity assumption, and the assumption that winds are forced only through these two mechanisms, the forcings as applied to the model should be able to reproduce the observed surface wind field. If this is so, then investigating the relative roles of elevated and surface heating is simply a matter of running the model with each forcing alone, and assessing the response of each. In practice, there are other forcings on the surface wind, for example, the possible forcing of the subtropical high from the extratropics. Thus, we focus our attention only on those regions where the wind field is highly correlated with the EOF time series.

b. Experimental cases

We apply our test to two dominant patterns of interannual climate variability, one for the tropical Pacific, and the other in the tropical Atlantic.

1) TROPICAL PACIFIC

We compute the combined EOF of monthly wind, precipitation, and SST anomalies from January 1979 to December 1998 over the tropical Pacific basin (20°N–20°S, 120°–280°E). The data grid spacing was 2.5° lat $\times$ 2.5° long. In this computation, points over land are excluded for the wind and SST fields, but included in the precipitation field. The winds, precipitation, and SSTA regressed from the EOF time series are shown in Figs. 1a,b. The pattern, which explains 23.2% of the variance, is typical of the mature phase of ENSO peaking around January. We also show the correlation of the zonal and meridional wind fields with the EOF time series (Figs. 1c,d). For zonal wind, the correlation is largest in the central equatorial Pacific and over the Indonesian subcontinent. For meridional wind, the largest correlations occur over the South Pacific convergence zone (SPCZ) region and over the Northern Hemisphere trades. Note that in the model runs, we apply forcing over the entire globe since there is the possibility of remote forcing. This is probably not an issue for surface forcing, but is definitely an issue for elevated heating.

2) TROPICAL ATLANTIC

We compute the combined EOF of monthly wind, precipitation, and SST anomalies from January 1979 to December 1998 over the tropical Atlantic basin (20°N–20°S, 70°W–20°E). The data grid spacing was 2.5° lat $\times$ 2.5° long. As before, points over land are excluded from the computation for the wind and SST fields, but included in the precipitation field. The winds, precipitation, and SSTA regressed from the EOF time series are shown in Figs. 2a,b. This pattern, which explains 12.4% of the variance, is associated with the tropical Atlantic ''dipole mode'' centered on March–May (MAM), with the characteristic cross-equatorial winds, dipole SSTA, and the ITCZ shift (Hastenrath and Greischar 1993). There is a fairly strong projection of precipitation heating in the eastern equatorial Pacific (not shown), but the correlation is weaker (in the 0.2–0.4 range). The projection is large simply because there is a lot of variance there. The correlation of the time series with the wind field (Figs. 2c,d) shows that the dominant wind signal is in the northern subtropics and the equatorial Atlantic region.

The forcing fields from the EOF are interpolated linearly onto the model grid. The model is integrated with a 0.5-day time step, and over 20 model days. At this point a quasi-steady state is reached. Our GCM results are the winds taken at day 20.

c. Tuning

We have eight tunable parameters:

- b, which controls the level of heating maximum; $(-1, 1)$
- σ_B, which defines the lower boundary of the heating; (0.6, 1)
- σ_{BL}, the thermal PBL height; (0.70, 0.95)
- r_{BL}, the thermal PBL relaxation rate; (1/2, 1/0.5) day^{-1}
- c, the vertical eddy viscosity coefficient; (0.1×10^{-7}, 3×10^{-7}) s^{-1}
- Y, the effective exchange coefficient (0.5×10^{-6}, 3×10^{-6}) s^{-1}
- r_N, the Newtonian cooling rate; (1/50, 1/10) day^{-1}
- r_{FMAX}, the free atmosphere Rayleigh damping rate; (1/20, 1/0.25) day^{-1}

The values in brackets correspond to the range over which the parameter value is searched. The range is based on physically plausible values: for example, the Newtonian cooling timescale is thought to be on the order of 1 month. For each of the tropical Pacific and Atlantic cases above, the model is run with both elevated heating and surface forcing, and the output field evaluated against the observed field. The cost function defining the goodness of fit is taken to be

$$C(u_{nz}, v_{nz}, r_u, r_v) = \sum_{|r_u|>0.4} |r_u|(u_{nz} - u_{NCEP})^2 + \sum_{|r_v|>0.4} |r_v|(v_{nz} - v_{NCEP})^2, \quad (6)$$

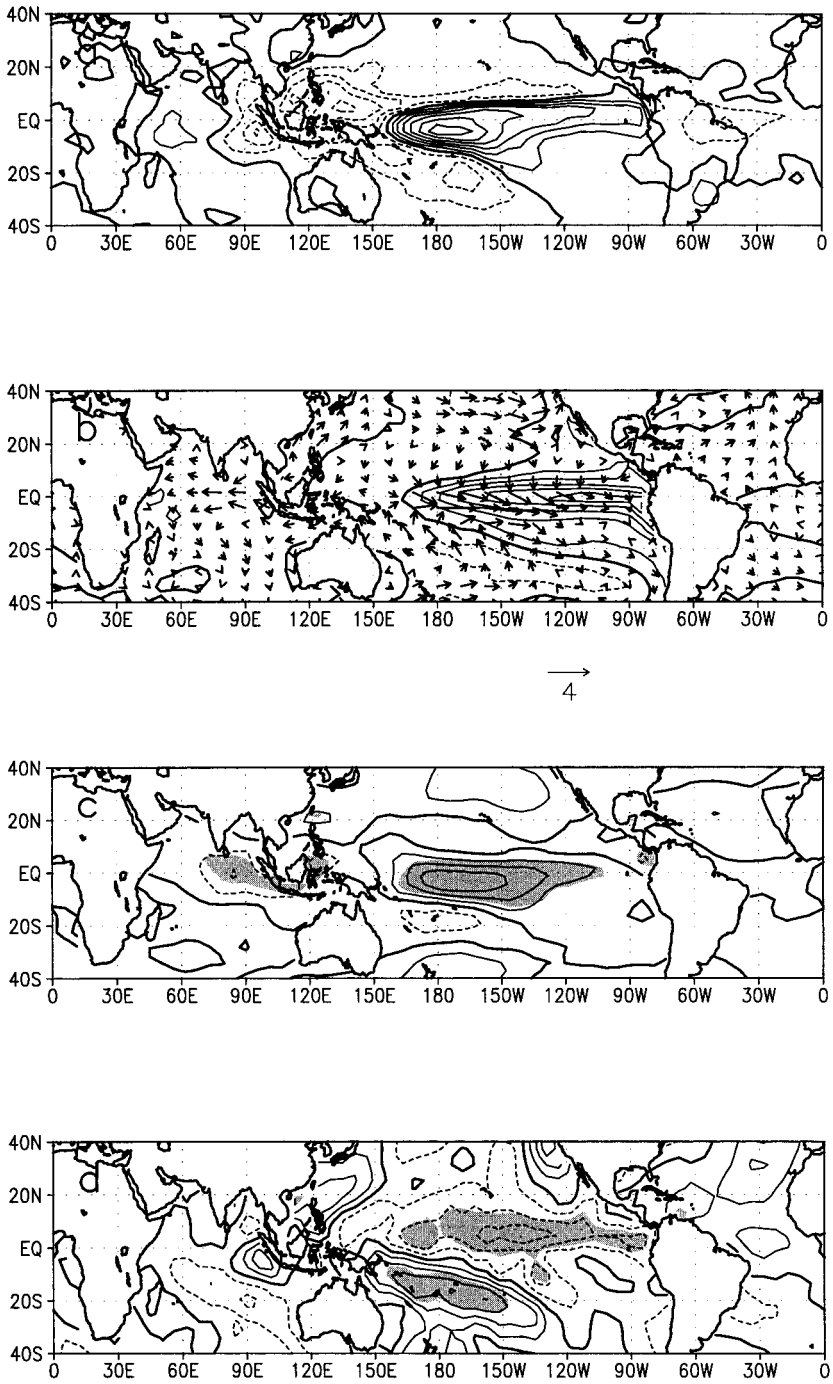

FIG. 1. Fields derived from the multivariate EOF for the tropical Pacific. (a) Precipitation [contour interval (CI) 1 mm day^{-1}]. (b) The 975-mb winds (reference wind is 4 m s^{-1}) and SSTA (CI 0.5 K). (c) Zonal wind (CI 1 m s^{-1}); shaded regions are where magnitude of the correlation exceeds 0.4 (d) Same as (c) but for meridional wind (CI 0.4 m s^{-1}). For all contour plots, the thick line represents zero and dashed lines represent negative values.

where the sum is taken over all grid points where the correlation of the time series with the wind field component r_u, r_v is larger than 0.4, provided that the latitude is within 12° from the equator. Our decision to limit the latitude range of the comparison was motivated by the physical limitations of our model. The model cannot account for transient eddy processes that may be significant to the surface momentum balance poleward of ~15°N and S (Murphree and van den Dool 1988); and furthermore we found the model to be incapable of ob-

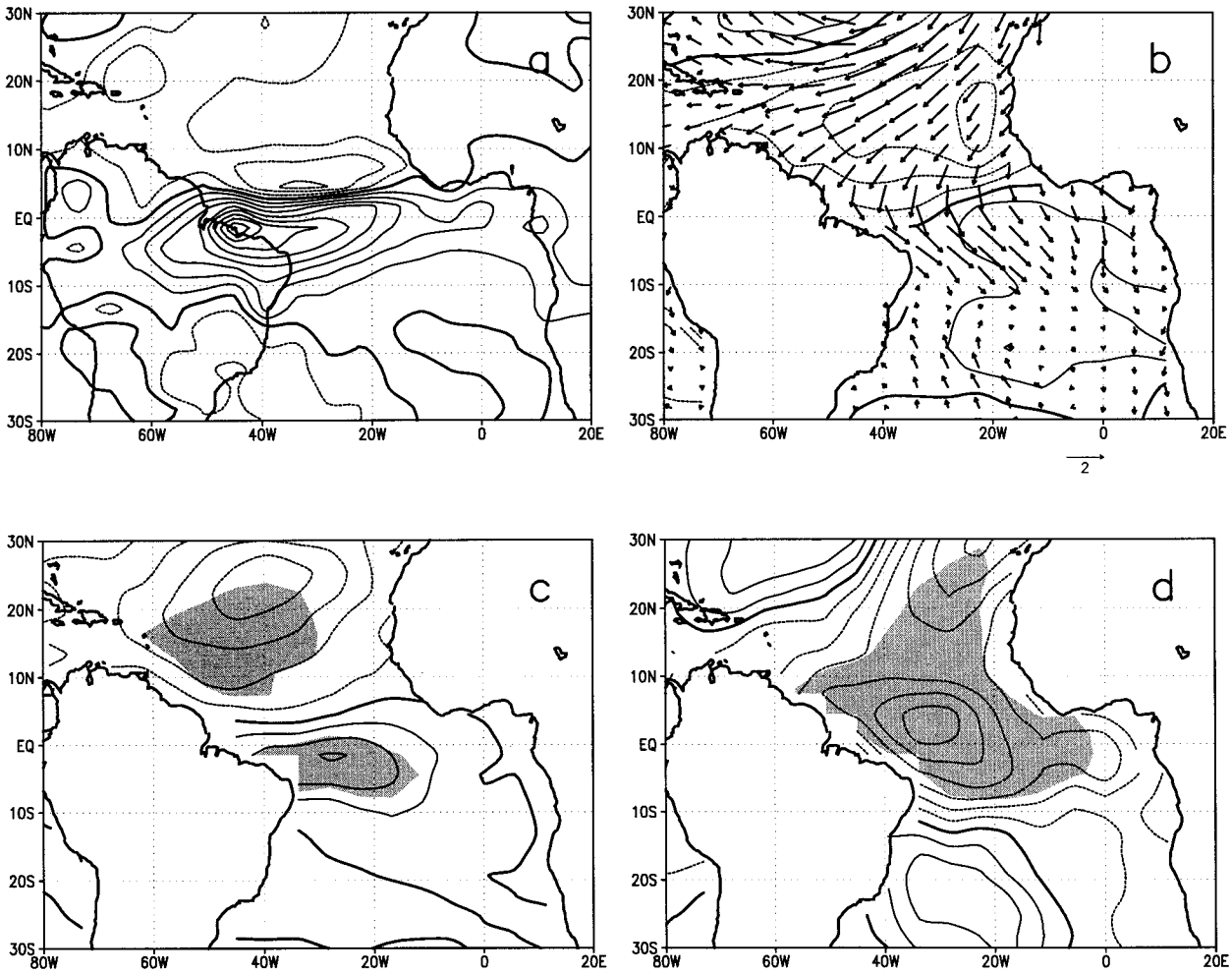

FIG. 2. Same as Fig. 1 but for the tropical Atlantic case. The contour intervals are (a) 0.5 mm day^{-1} for precipitation, (b) 0.3 K for SST, (c) 0.5 m s^{-1} for zonal wind, and (d) 0.25 m s^{-1} for meridional wind. The reference wind vector in (b) is 2 m s^{-1}.

taining realistic anomalous wind magnitudes for our tropical Atlantic case north of ~12°N, suggesting either missing physics, or complications in the link between the observed winds and forcings (see section 8). We did try an optimization taking the latitude range considered out to 18°N and S, but the tuning for that case did not give a better model simulation for the subtropical North Atlantic surface winds. Finally, the cost at each grid point is weighted by the absolute value of the correlation, allowing grid points with higher correlation to have more influence on the outcome. The procedure is repeated, with different parameters, until an acceptable minimum is reached. The algorithm used for searching the minimum is the downhill simplex method of Nelder and Mead (1965), as implemented in Matlab (fmins.m). While computationally not very efficient, the method is simple to implement and use.

The optimization is done concurrently with both the tropical Pacific case and the tropical Atlantic case contributing toward a joint cost function, which is in our case just the sum of the two individual cost functions defined by (6) above. In other words, for each iteration of the simplex method, the tropical Pacific case is run with its given set of parameters, and concurrently the tropical Atlantic case is run with its given set of parameters. The cost function returned is the sum of the individual cost functions for each of the two runs. As far as the parameters are concerned, we allow parameters directly controlling the heating profile (b and σ_B) to evolve independently for the tropical Pacific and tropical Atlantic cases. We expect the elevated heating parameters to differ, since the profile of ITCZ heating (characterizing the tropical Atlantic situation) and the warm pool heating (characterizing the tropical Pacific case) are different. The other parameters—the thermal PBL height and damping rate (σ_{BL}, r_{BL}), the boundary layer momentum diffusion parameters (c, Y), the troposphere Raleigh damping rate (r_{FAM}),and the radiative relaxation rate (r_N)—are shared between the two cases as we do not expect them to differ substantially from one region to the next.

Table 1 shows the optimal values for each case. The

TABLE 1. The optimal parameters used for each experimental case. Column 1: tropical Pacific case. Column 2: tropical Atlantic case. Column 3: tropical Pacific case, with only surface forcing.

Parameter (values in brackets are the search limits)	Tropical Pacific	Tropical Atlantic	Tropical Pacific (LN only)
b (controls peak of heating) (−1, 1)	1.00	0.175	N/A
σ_B (lower limit of heating) (0.6, 1)	0.72	1.00	N/A
c (vertical viscosity) (0.1×10^{-7}, 3×10^{-7}) s^{-1}	0.95×10^{-7} s^{-1}	0.95×10^{-7} s^{-1}	0.21×10^{-7} s^{-1}
Y (exchange coefficient) (0.5×10^{-6}, 3×10^{-6}) s^{-1}	1.0×10^{-6} s^{-1}	1.0×10^{-6} s^{-1}	0.5×10^{-6} s^{-1}
r_N (Newtonian damping rate) (1/50, 1/10) day^{-1}	1/16.3 day^{-1}	1/16.3 day^{-1}	1/10.1 day^{-1}
σ_{BL} (thermal PBL height) (0.7, 0.95)	0.725	0.725	0.713
r_{BL} (thermal PBL relaxation rate) (1/2, 1/0.5) day^{-1}	1/1.16 day^{-1}	1/1.16 day^{-1}	1/1.89 day^{-1}
r_{FMAX} ('free' atmosphere Rayleigh damping rate) (1/20, 1/0.25) day^{-1}	1/3.58 day^{-1}	1/3.58 day^{-1}	1/20.0 day^{-1}

Pacific case shows a preference for the elevated heating source to peak at a higher level, relative to the Atlantic case. We discuss the relevance of this difference in section 7. The thermal boundary layer height at $\sigma = 0.725$ is somewhat higher than the observed range of PBL heights over the tropical oceans (around 800–950 mb) and possibly indicates a model deficiency. In this regard, we note that LN used a 3-km (~700 mb) PBL height, although the reduced gravity model of Battisti et al. (1999) brought this down to a more realistic 1.5–2-km level. We discuss possible model deficiencies in section 8. As it stands, using a higher than observed thermal PBL height exaggerates somewhat the influence of the surface forcing mechanism in our model (see section 7e).

5. Model results

a. Tropical Pacific

The simulated wind field for the optimally tuned case is shown in Figs. 3a–c, to be compared with the observed field in Figs. 1b–d. (Note: the contours in Fig. 3a are model temperature anomalies at 975 mb, and not of surface temperature as in Fig. 1b. This is also the case for panel a of Figs. 4–9.) Not surprisingly, the model 975-mb anomalous temperature follows closely the imposed surface temperature anomaly, and is consistent with the LN assumption of a well-mixed thermal boundary layer. All large-scale structures of the zonal and meridional wind in the high-correlation regions (shaded regions of Figs. 1c,d) are captured by the model, and with approximately the correct magnitudes. Some of the finer details are not captured however, most notably the structure of the meridional winds in the central and eastern Pacific. The model captures other prominent structures poleward of 12°N and S or that did not exceed the $r = 0.4$ correlation threshold (and hence were not included in the computation of the cost function): the meridional winds in the SPCZ region, the anomalous easterlies south of the westerly maximum in the Central Pacific, the anomalous northerlies over the south tropical Indian Ocean, and the weak southerlies in the cold tongue region. The magnitudes of the model response in these regions are comparable to observations, except that the model southerlies in the cold tongue region are a bit too strong.

Comparison of the 975-mb divergence field (not shown in figure) shows that, in the cold tongue region, the magnitude of the equatorial convergence is slightly larger in the model fields, and the divergence to the south of it is also somewhat too large. Also, the convergence in the central Pacific near the dateline is somewhat deficient in the model. However, the large-scale structure of the model divergence field generally compares quite well to the observed. We conclude that the model gives a decent representation of the observed winds, and we proceed with running the two cases of individual forcing.

The run with convective-only forcing (Fig. 4) shows a similar zonal wind structure as the run with full forcing. Noticeable differences are in the magnitude of the westerlies in the central Pacific, which is a little bit weaker in the convective-only case, and also in the structure of these westerlies, which is meridionally broader to the east of the date line in the convective-only case. The meridional wind structure shows greater differences. Most significantly, the northerlies in the cold tongue region are missing in the convective-only case, whereas there is a band of northerlies northeast of the SPCZ region, the maximum amplitude around 0.6 m s^{-1}. However, the southerlies in the SPCZ region, and the northerlies in the south tropical Indian Ocean, are similar in both structure and magnitude. Also, the northerlies in the subtropical North Pacific are of the similar magnitude in the convective-only and full runs, although the correspondence in structure is less certain.

The discrepancy between the convective-only and full forcing cases is accounted for by the surface forcing case (Fig. 5). Surface forcing contributes little to the zonal wind response; it has weak easterlies in the eastern Pacific in the northern and southern subtropics, and weak westerlies (~0.5 m s^{-1}) in the equatorial region near the date line. The meridional wind exhibits a dipolelike structure with northerlies (maximum ~1.2 m s^{-1}) to the north of the maximum SSTA in the eastern equatorial Pacific, and somewhat weaker southerlies (maximum ~0.6 m s^{-1}) to the south. The northerlies constitute the bulk of the ITCZ response seen in the full

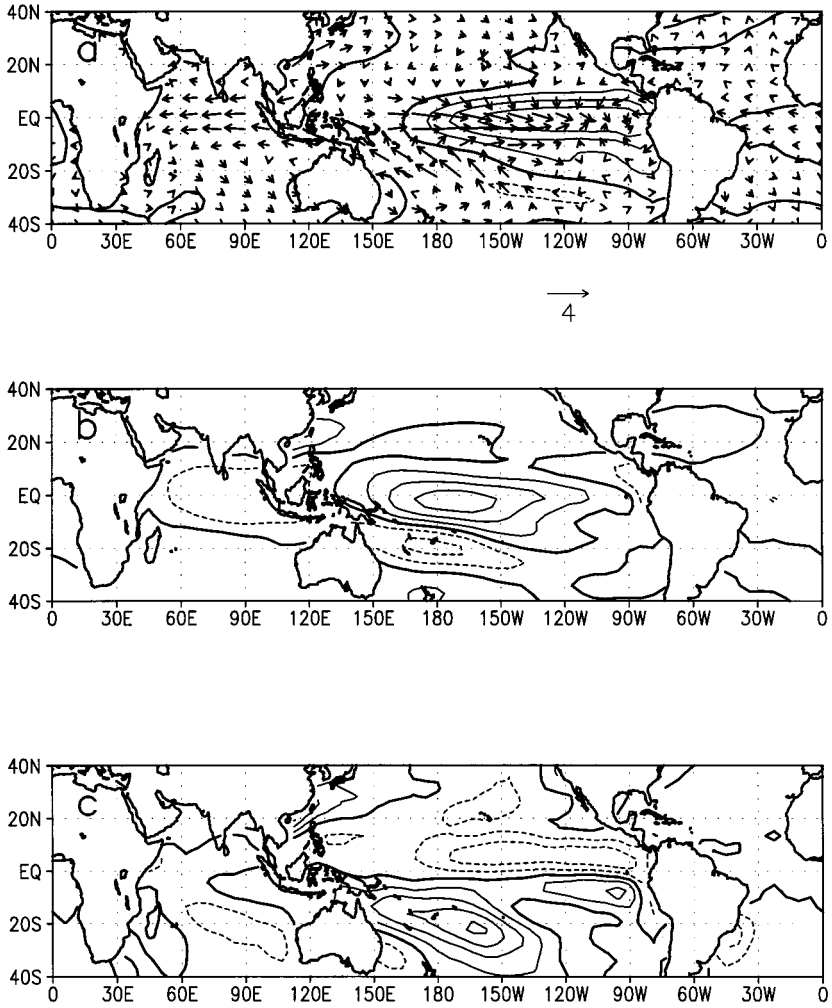

FIG. 3. Wind fields as generated by the model for the tropical Pacific case: (a) 975-mb winds. The contours are model 975-mb temperature anomalies (CI 0.5 K). (b) Zonal wind. (c) Meridional component. Note that the contour intervals and/or reference wind vector for Figs. 3a–c are the same as for Figs. 1b–d, respectively.

forcing case, whereas much of the southerlies to the south of the maximum SSTA are cancelled by the northerlies generated by the elevated heating.

An interesting feature is the anomalous temperature response at the lowest model level. The bulk of the response comes from surface forcing; elevated heating contributes little to the temperature anomalies at the lowest model level. Also, surface forcing accounts for virtually all of the convergence in the equatorial cold tongue region (not shown in figure), whereas elevated heating accounts for the bulk of the convergence/divergence seen in the SPCZ region between 8°S and 25°S, and between 160°E and 130°W.

In summary: the model wind fields compare well with the observed wind fields. In the model, elevated heating is responsible for most of the zonal wind, and for the meridional wind in the SPCZ and subtropical regions. Surface forcing is the dominant contributor to the meridional wind response in the large SSTA gradient region of the eastern equatorial Pacific.

b. Tropical Atlantic

The simulated wind field is shown in Fig. 6, to be compared with the observed field in Figs. 2b–d. The correspondence in structure and magnitude between model and observed in the high-correlation region is not nearly as good as in the tropical Pacific case. The model zonal winds clearly obtain the westerlies in the equatorial region, and the easterlies in the northern subtropics. However, the magnitudes are off: the westerlies at the equator near the coast of South America are too large ($\sim$1.5 m s^{-1} as opposed to 1 m s^{-1} observed), and the easterlies in the northern subtropics are too weak (0.5 m s^{-1} as opposed to 1–1.5 m s^{-1} observed). The meridional winds do slightly better: anomalous north-

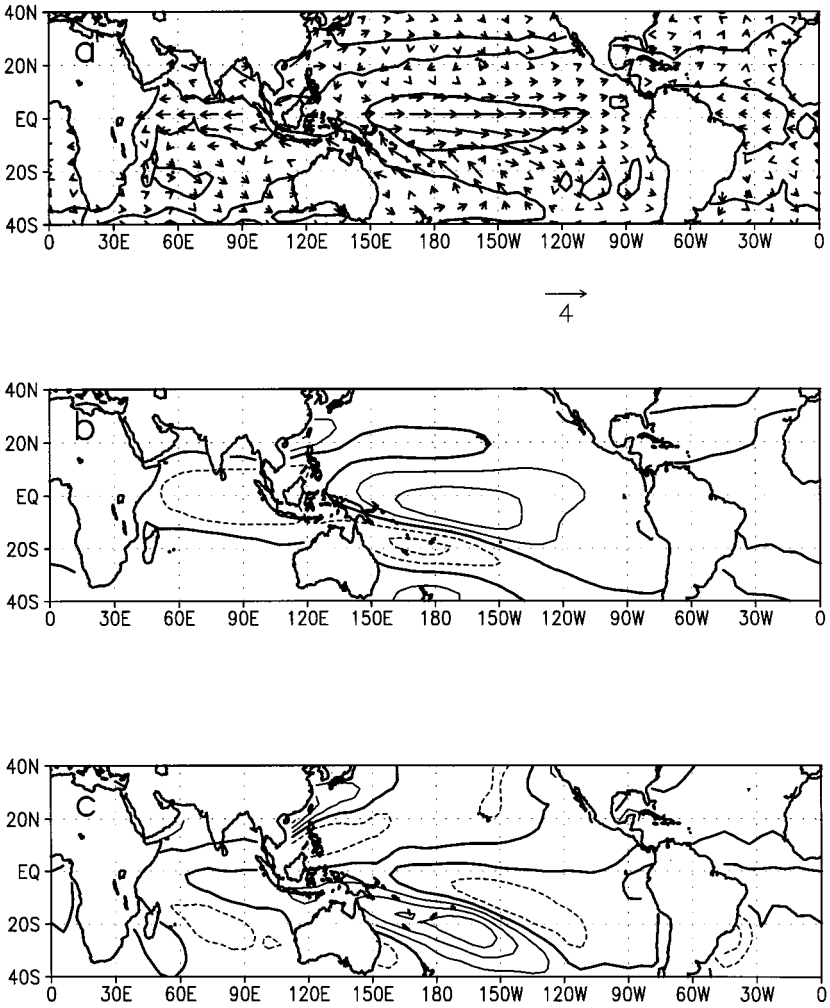

FIG. 4. Same as Fig. 3 but for elevated heating only.

erlies dominate the model response in the northern subtropics and equatorial region, and southerlies occur in the South Atlantic convergence zone (SACZ) region, in accordance with the observed field. However, the model's anomalous northerlies are too weak in the northern subtropics. Furthermore, the detailed structure of the meridional wind does not correspond well. For example, maximum northerlies occur around 2.5°N, 30°W in the observed, whereas in the model it occurs around 4°N, 25°W. The divergence fields (not shown in figure) get the large-scale divergence to the north of 3°N and convergence to the south in accordance with observations, but the details of the structure are not well simulated. In particular, the model has a maximum in convergence just south of the equator (~3°S) around 22°W, with a magnitude 1.5 times that observed; whereas the observations show the largest convergence occupying a band running roughly east to west between 5°S and 10°S. We proceed with the runs with individual forcing, but keeping mindful that the model winds are not as realistic as for the tropical Pacific case.

The case with elevated heating (Fig. 7) shows that it is responsible for the bulk of the zonal wind response, similar to the tropical Pacific case. This appears also to be the case for zonal wind in the northern subtropics. Elevated heating also dominates the subtropical meridional wind response; it produces the bulk of the southerlies in the SACZ region, and the northerlies in the northern subtropics. Surface forcing (Fig. 8) dominates the meridional response near the equator, producing northerlies (0.5–1 m s^{-1}) in the equatorial region where the cross-equatorial SST gradients are strong. However, elevated heating does contribute to the meridional winds near the equator, especially in the western Atlantic where the magnitude exceeds 0.5 m s^{-1}. The zonal wind response for the surface-forcing-only run is small: the only significant contribution is the weak easterlies in the north tropical Atlantic.

As with the tropical Pacific case, surface forcing contributes the bulk of the lowest level anomalous temperature response. It also contributes to the larger fraction of the 975-mb model divergence, although there is

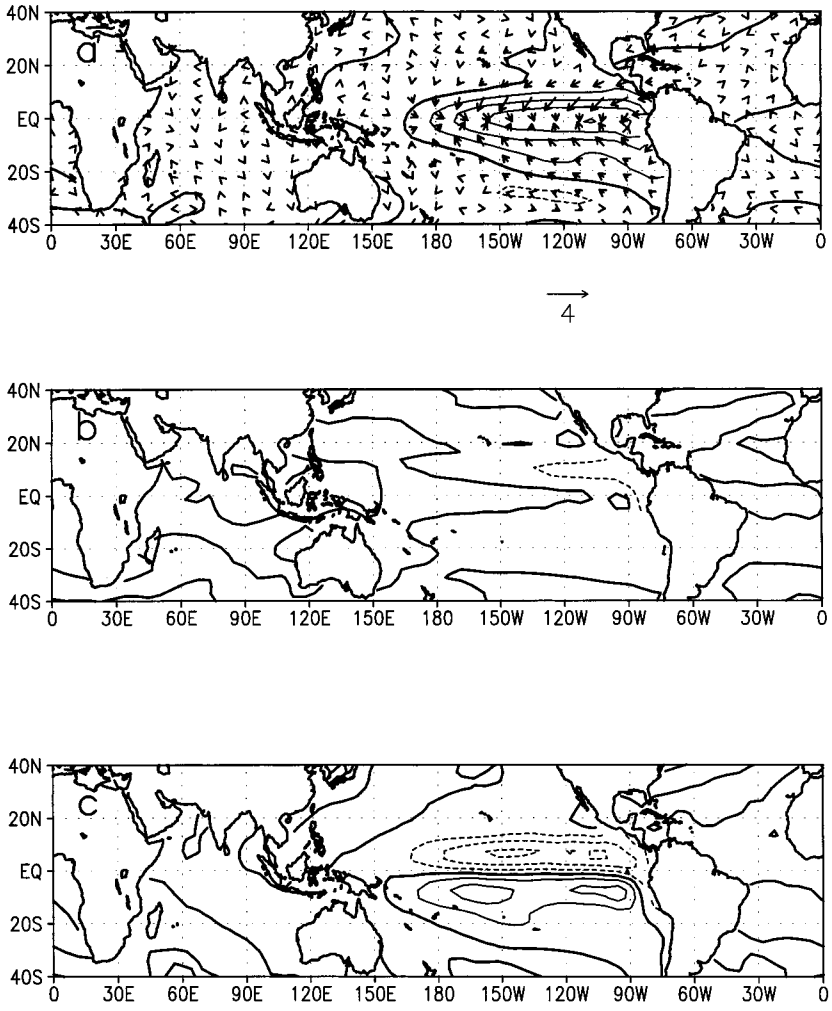

FIG. 5. Same as Fig. 3 but for surface forcing only.

a significant contribution by elevated heating in the western half of the basin, just south of the equator.

In summary: the model wind fields with full forcing have structure similar to the observed fields, although the model winds are too weak in the northern subtropics. Our results here regarding the relative roles of the two forcings are similar to the Pacific case: elevated heating generates the bulk of the zonal wind response, as is the bulk of the meridional wind response in the SACZ region. It also explains a larger part of the northern subtropical wind response. In the strong SSTA gradient region near the equator, surface forcing is the dominant contributor to the meridional wind response.

c. A surface forcing-only tuned model

The results above suggest a greater role for elevated heating in forcing zonal wind everywhere in the Tropics, and meridional wind in the subtropics; and a greater role for surface heating in forcing meridional wind near the equator. We further demonstrate the validity of this result by optimizing the model for the tropical Pacific case, but only with the surface forcing present. The point of this exercise is to show that no realistic choice of parameter settings for the surface-forcing-only model can account for the zonal wind response, and meridional wind response away from the equator. Table 1 shows the optimized parameters derived from the tuning. Note that several parameters—namely the Newtonian cooling rate, the effective exchange coefficient, and the Rayleigh damping rate—reached a limit of their search range. The model fields (Fig. 9) are similar to the surface-forcing-only case computed in section 5a (Fig. 5), with strong meridional wind response in the central and eastern equatorial Pacific. The westerlies in the equatorial band near the date line are stronger than that for Fig. 5, but nowhere near as strong as in observations.

6. Model verification

To test the wider applicability of the model and its particular set of tuned parameters, we attempt two ad-

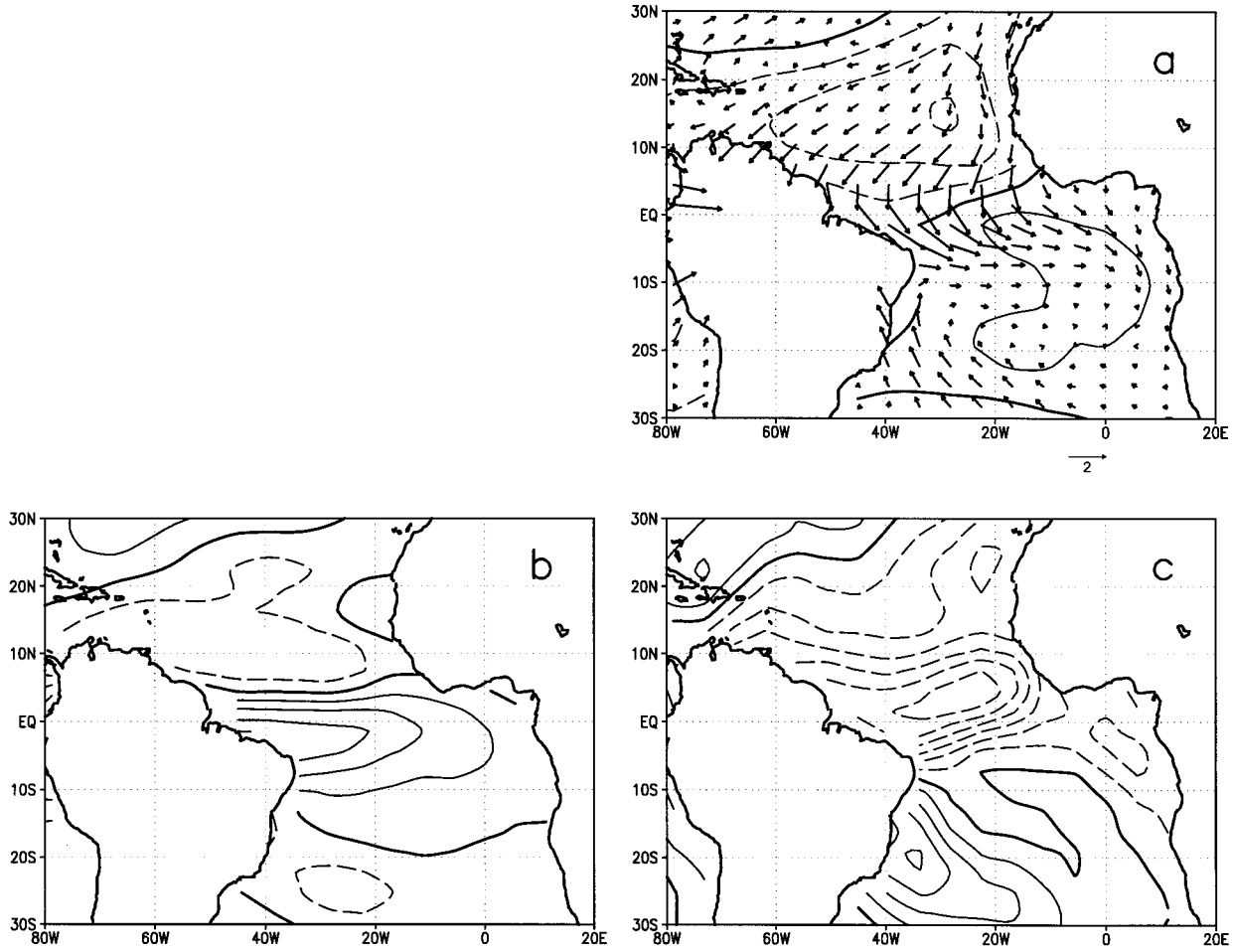

FIG. 6. Wind fields as generated by the model for the tropical Atlantic case: (a) 975-mb winds. The contours are model 975-mb temperature anomalies (CI 0.5 K). (b) Zonal wind. (c) Meridional wind. Note that the contour intervals and/or reference wind vectors for (a)–(c) are the same as for Figs. 2b–d, respectively.

ditional simulations: i) a June–August (JJA) climatological eddy (in this section we use ''eddy'' to mean deviation from the zonal average) simulation; and ii) a month-by-month simulation of anomalous wind fields using the 20 yr of precipitation and SST data available.

a. Climatological JJA eddy simulation

We use climatological eddy JJA precipitation and SST as forcing on the model. Note that LN originally demonstrated their model using eddy fields. As with LN, we focus on the tropical Pacific, and use the same parameters as found from tuning the tropical Pacific case above.

Figure 10a shows the NCEP–NCAR 975-mb eddy JJA fields, to be compared with model 975-mb fields in Fig. 10b. Much of the tropical flow is reproduced in the model: the trades in the northern Pacific (and also the Atlantic) Tropics are of comparable strength and orientation to the real winds, and the southerlies over the South China Sea are also reproduced. However, the model southeasterly trades are somewhat too zonal in orientation. A major discrepancy in the tropical flow is the cross-equatorial flow related to the Indian monsoon, which is absent in the model simulation despite the significant diabatic heating over the Indian subcontinent and the presence of orography in the model.

We break the model flow down to its elevated heating and surface temperature gradient contributions (Figs. 10c,d). The larger part of the 975-mb wind structure in the simulation with full forcing is reproduced in the elevated heating-only run. The surface forcing contributes mainly to the northeasterly trades in the central Pacific.

The presence of flow features distinguishes those features that respond linearly to thermal sources from flow that is driven by other forcing or depends on nonlinear dynamics. We mentioned previously the lack of cross-equatorial winds in the Indian Ocean. Also visibly lacking is the surface midlatitude flow, which is tied to the baroclinically unstable midlatitude dynamics.

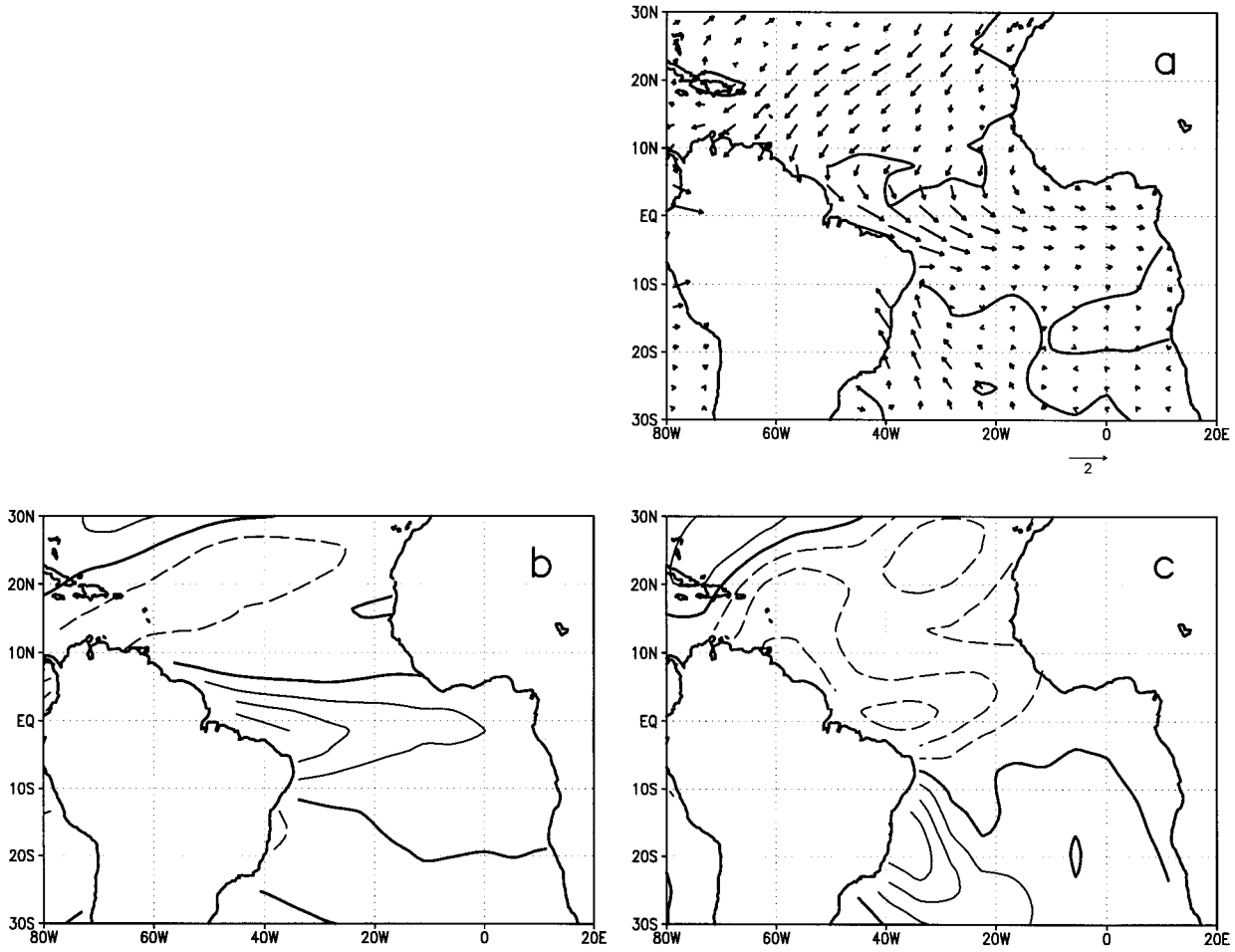

FIG. 7. Same as Fig. 6 but for elevated heating only.

b. Long-term monthly simulation

We compute monthly anomalous wind fields for the period January 1979–December 1998, using monthly anomalous precipitation from the Xie and Arkin (1997) dataset, and NCEP–NCAR SST anomalies. We use the same model tuning as for the tropical Pacific case above, and hence we focus our comparison with observations to the Pacific and western Indian Ocean basins. The anomalies are computed in real time, evolving the forcings over time through linear interpolation (in time) of the monthly forcing fields. For simplicity we assume that each month contains 30 days. The model surface winds are sampled once a day and averaged to form monthly means.

We assess the model output by correlating the 975-mb model wind components with the NCEP–NCAR 975-mb anomalous wind components (Fig. 11). Most of the correlation above 0.4 resides over the tropical oceans, as expected. The tropical Atlantic winds appear less well simulated, which is expected since we use the model tuning for the tropical Pacific case. There is surprising correlation with wind fields in the North Atlantic; however, the midlatitude anomalous wind generated by the model is much smaller compared to the observed. The highest regression values (above 0.6) for zonal wind occur over the central and northeastern tropical Pacific; and for meridional wind (above 0.5) over the SPCZ region, the northeastern tropical Pacific and the eastern Pacific regions.

A prominent failure of the model is winds over the subtropical west coasts of the Americas (and also over Africa). We note the coincidence of these areas with regions containing stratus cloud decks, and postulate an influence of the stratus cloud on surface winds (see section 8b).

7. Sensitivity studies

a. Role of the heating profile

A prominent difference between the two cases of forcing is the elevated heating profile (Fig. 12). The Pacific case has its peak at virtually the maximum possible height as allowed by the parameterization, whereas the Atlantic profile has its peak around 600 mb, characteristic of the lower ITCZ heating. This is in qualitative

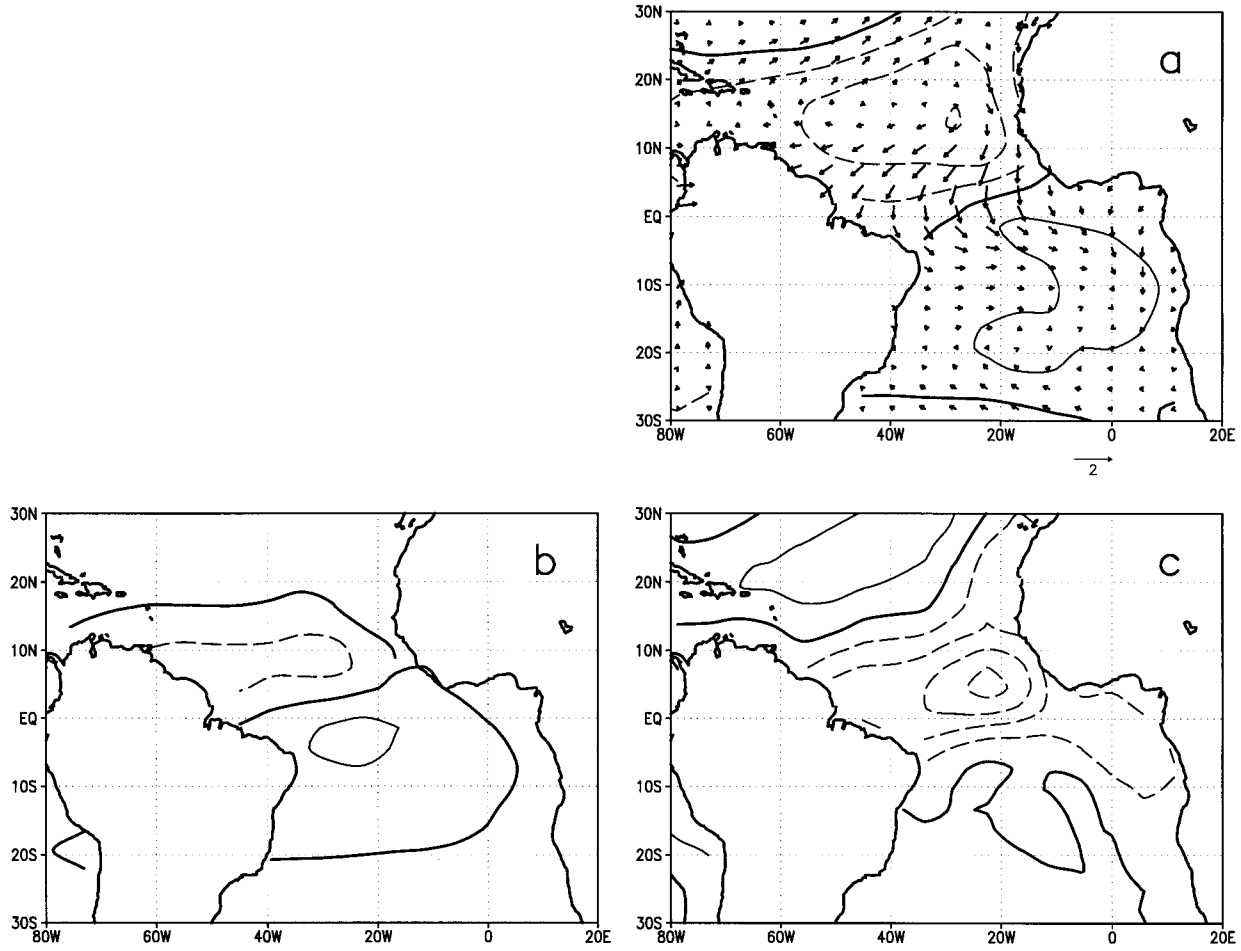

FIG. 8. Same as Fig. 6 but for surface forcing only.

agreement with heating profiles of cumulus convection as documented by Thompson et al. (1979), where they show West Pacific profiles peaking around 450 mb, whereas East Atlantic heating peaks much lower at around 700 mb. We demonstrate the sensitivity of the surface wind response to heating profile by integrating the Pacific and Atlantic cases again with the tuned parameter values, but with the heating profile parameters b and σ_B exchanged (so that the Pacific case has the Atlantic case heating profile and vice versa). The Pacific case (not shown) has similar structure to before, but with the wind magnitudes significantly larger—up to twice as large for the zonal wind anomalies near the equator. Northerlies in the ITCZ region double (to ~2 m s^{-1} compared to ~0.9 m s^{-1} in the original), and similarly for the southerlies in the SPCZ region. By comparison, meridional winds for the Atlantic case (not shown) weaken in both the equatorial and SACZ region by around 0.5 m s^{-1}, likewise for the westerlies near the equator.

In short, surface wind in the vicinity of elevated heating anomalies increase (decrease) as the heating profile is lowered (raised). We think this arises because heating profiles with lower heating project more strongly on higher modes that have significant amplitude at the surface (cf. Wu et al. 1999b).

b. Role of the Ekman boundary layer

We highlight the role of the Ekman boundary layer in a tropical Pacific case run with the exchange coefficient Y set to zero. There is no surface momentum flux, and a free-slip condition holds at the surface. However, momentum diffusion in the interior of the model atmosphere still occurs.

The Ekman layer plays a crucial role in attenuating the surface expression of zonal wind. The 975-mb zonal winds of this run show substantial increase in the westerlies of the central Pacific—9 m s^{-1} as compared to 3–4 m s^{-1} for the case with surface flux. Also, the peak of the westerlies shifts westward to around the date line. The vertical profile of zonal wind at the date line on the equator (Fig. 13a) for the no flux and flux conditions demonstrate the attenuation in the boundary layer. However, the magnitude and structure of the 975-mb meridional wind remains roughly similar to before. The ver-

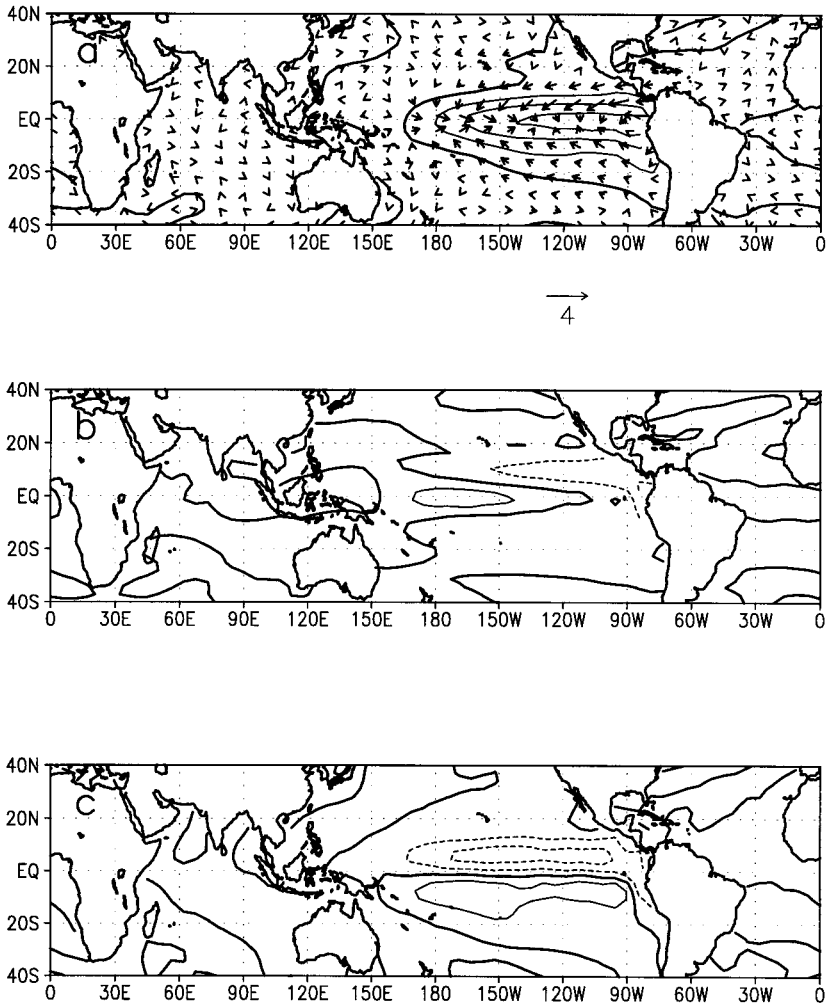

FIG. 9. Same as Fig. 3 but for the surface-forcing-only tuned model run.

tical profile of meridional wind in the ITCZ region of the eastern Pacific (Fig. 13b) shows that meridional wind in the boundary layer is affected, but only away from the surface. The wind profiles with surface flux are more realistic, since zonal wind is known to increase away from the surface in the boundary layer, and meridional wind magnitude near the boundary layer top is generally smaller than winds near the surface (Deser 1993).

The Ekman boundary layer also sets up the asymmetry in the linear friction coefficients of the surface wind momentum balance, a relationship first noted by Deser (1993) and elaborated by Chiang and Zebiak (2000). Deser found that the meridional friction coefficients are two to three times larger than the zonal friction coefficients and attributed this difference to the asymmetry to the winds at the top of the PBL, under the assumption of a diffusive Ekman boundary layer. Our model results support this view: in the case with surface momentum flux, the 975-mb winds obey an essentially linear relationship between the residual of the geostrophic balance, and the appropriate wind component (Figs. 14a,b). The friction coefficient—computed as the negative slope of the best-fit line through the points—shows that the meridional friction coefficient (2.04×10^{-5} s^{-1}) is between two and three times larger than the zonal friction coefficient (at 0.73×10^{-5} s^{-1}). Furthermore, the values of the friction coefficients are also comparable to those obtained from analysis of NCEP–NCAR surface winds (Chiang and Zebiak 2000). The run with zero surface momentum flux does not display the close relationship between the residual of the geostrophic balance and the wind components (Figs. 14c,d).

c. Role of topography

A tropical Pacific case run with no topography showed little difference from the ''standard'' tropical Pacific run, at least for the interior of the ocean basins. Zonal winds over tropical oceans tend to be more easterly, by $\sim$0.2 m s^{-1} over the tropical Indian and Atlantic

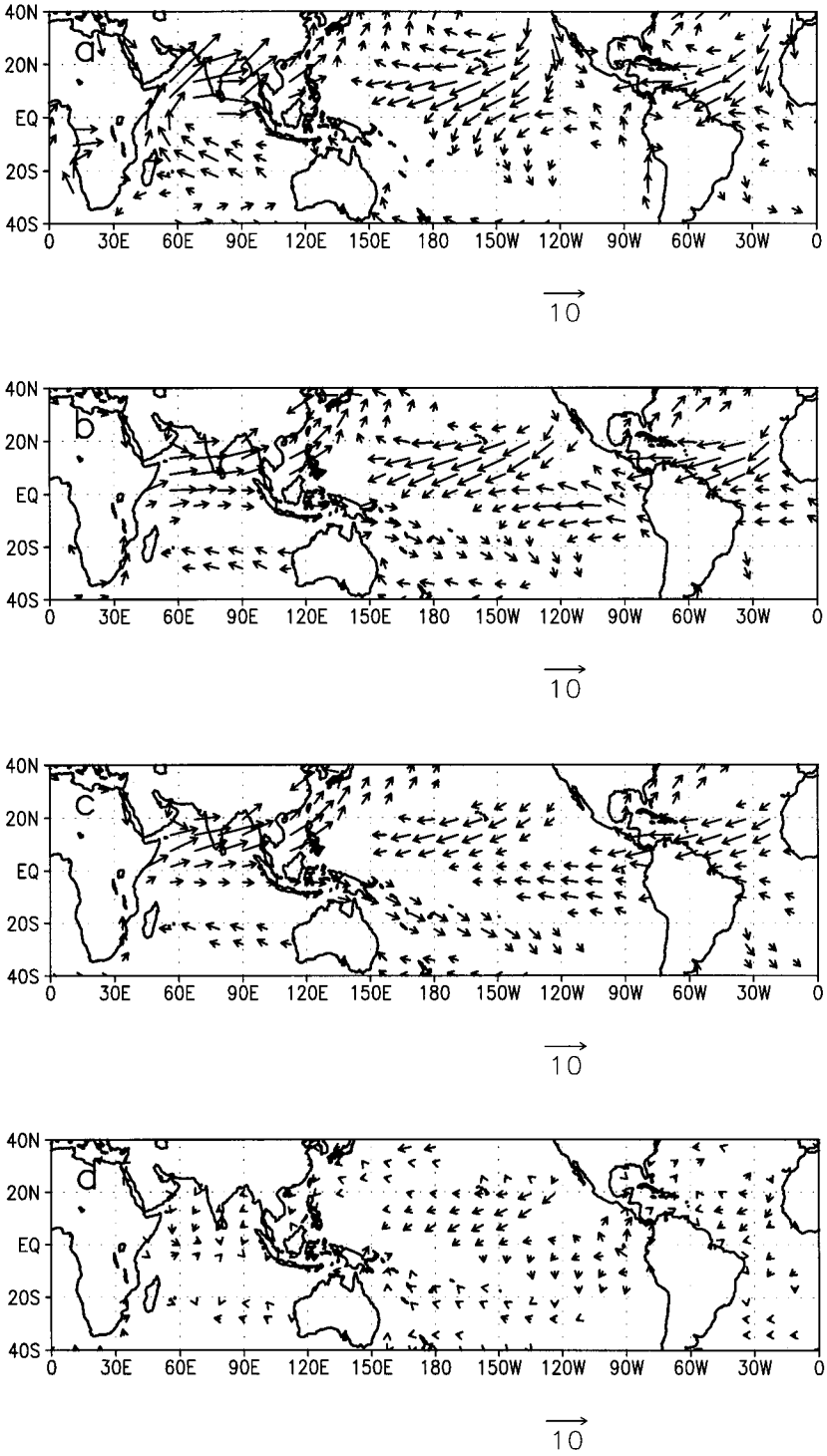

FIG. 10. (a) NCEP–NCAR 975-mb JJA eddy wind field. (b) Model-generated JJA eddy wind field. (c) Same as for (b) but with elevated heating only. (d) Same as (b) but with surface forcing only. Only wind vectors with magnitudes greater than 2 m s^{-1} are shown. The reference wind vector is 10 m s^{-1}.

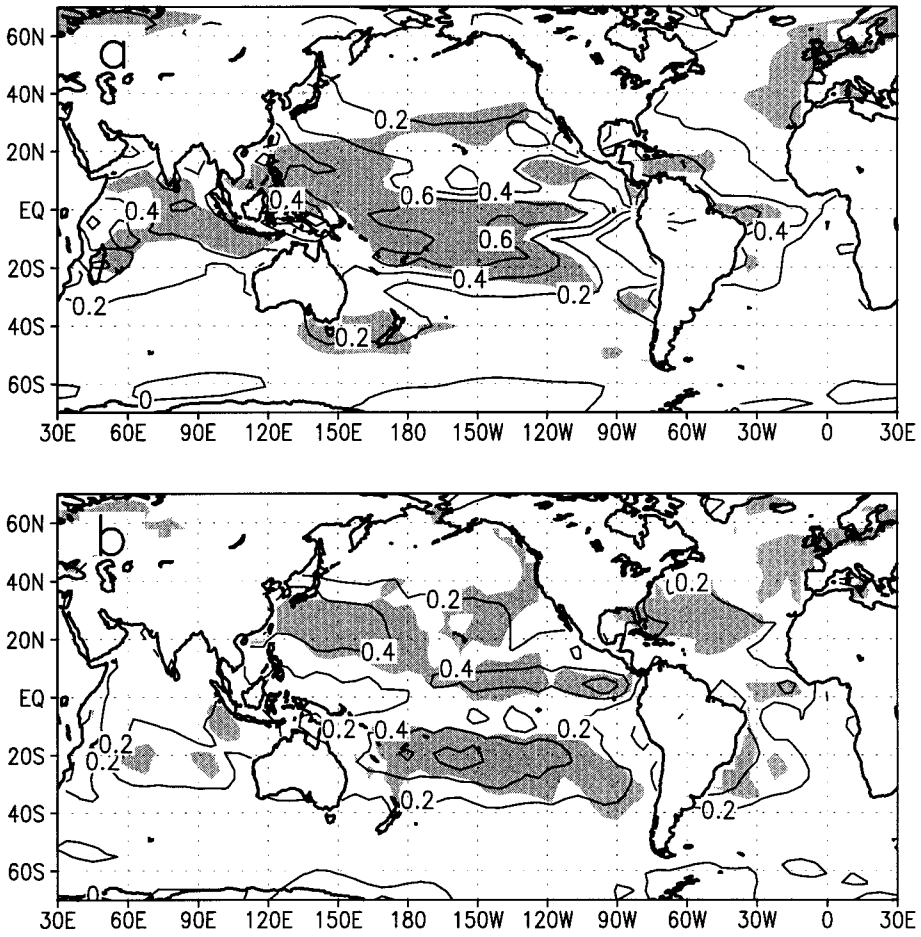

FIG. 11. Regression and correlation maps of the model monthly anomalous 975-mb wind (Jan 1979–Dec 1998) with NCEP–NCAR anomalous 975-mb winds. (a) Zonal wind. (b) Meridional wind. For each figure, the shading indicates regions where correlation exceeds 0.4, and contour values are a regression of the model winds on the NCEP–NCAR anomalous winds (CI 0.2).

Oceans, and by 0.2–0.8 m s^{-1} in the equatorial eastern Pacific, maximizing at the west coast of equatorial South America. There are strong localized changes of wind near coastlines in the SACZ region, the east coast of South America around 20°S, and off Southeast Asia. However, the significance of these changes is difficult to assess, as there is possible interpolation error (conversion from sigma to pressure surfaces) near coastlines. Furthermore, the model does not have the necessary horizontal resolution for resolving features like boundary currents or lee waves that are a feature of flow associated with topography.

d. Role of Newtonian damping

The model surface wind is not sensitive to change in the radiative relaxation rate, at least for factor of 2–4 increases. Running the model for the tropical Pacific case but with 1/8 day^{-1} rate instead of the usual 1/16.3 day^{-1} rate results in a maximum change in zonal winds of ~0.3 m s^{-1}, and ~0.1 m s^{-1} for meridional winds. The model wind structure remains essentially unchanged.

e. Role of the thermal PBL height and relaxation rate

We test the sensitivity of the PBL relaxation rate by executing two runs, one with relaxation rate twice as fast as the tuned tropical Pacific case (1/0.5 day^{-1}), and the other with relaxation rate half as fast (1/2 day^{-1}). The change is largest for the meridional winds in the eastern equatorial Pacific region. The faster damping rate increases the northerlies in the northeastern equatorial Pacific by around 0.4 m s^{-1} relative to the standard tropical Pacific case; the opposite occurs for the slower damping rate case. The response in the zonal wind is relatively small.

The thermal boundary layer height also has significant impact on the northerlies in the eastern equatorial Pacific. Lowering the PBL height by 0.1 σ units from its tuned position of 0.725 decreased the northerlies by ~0.4 m s^{-1}. This response is consistent with the de-

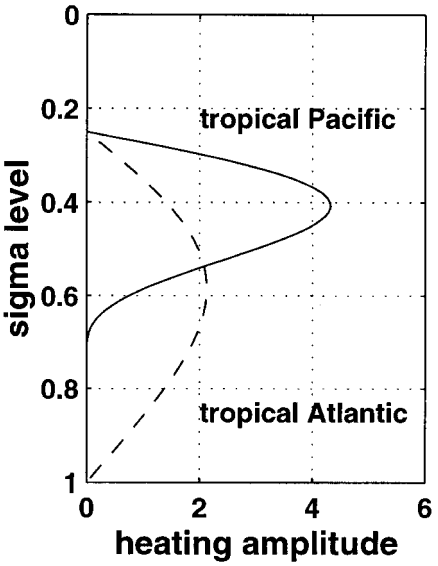

FIG. 12. Vertical profile of the imposed elevated heating for the tropical Pacific case (solid line) and the tropical Atlantic case (dashed line).

creasing strength of surface forcing as temperature perturbations occupy less atmospheric thickness. The change in zonal wind is also not small: the maximum equatorial westerlies near the date line reduce in magnitude by about 1 m s^{-1}, leading to a zonal wind structure somewhat similar to the results for the elevated heating-only case (cf. Fig. 4). This cause of the zonal wind change is primarily due to the reduction in the strength of surface forcing, which weakens with decreasing PBL height.

f. Role of the basic-state vertical temperature profile and PBL inversion

Finally, we tested the effect of a PBL inversion by altering the basic-state vertical temperature profile used to simulate an inversion in the vicinity of the PBL top. Increasing the inversion strength from the original profile to the modified profile (Fig. 15) decreased the zonal wind strength over the equatorial band (10°S–10°N) by ~20%, and the meridional wind response in the SPCZ region also by ~20%. However, meridional wind strength over the eastern equatorial Pacific *increased* by ~25%. Running the model with the modified profile with the individual cases of forcing shows that the elevated heating response *decreases* with increasing in-

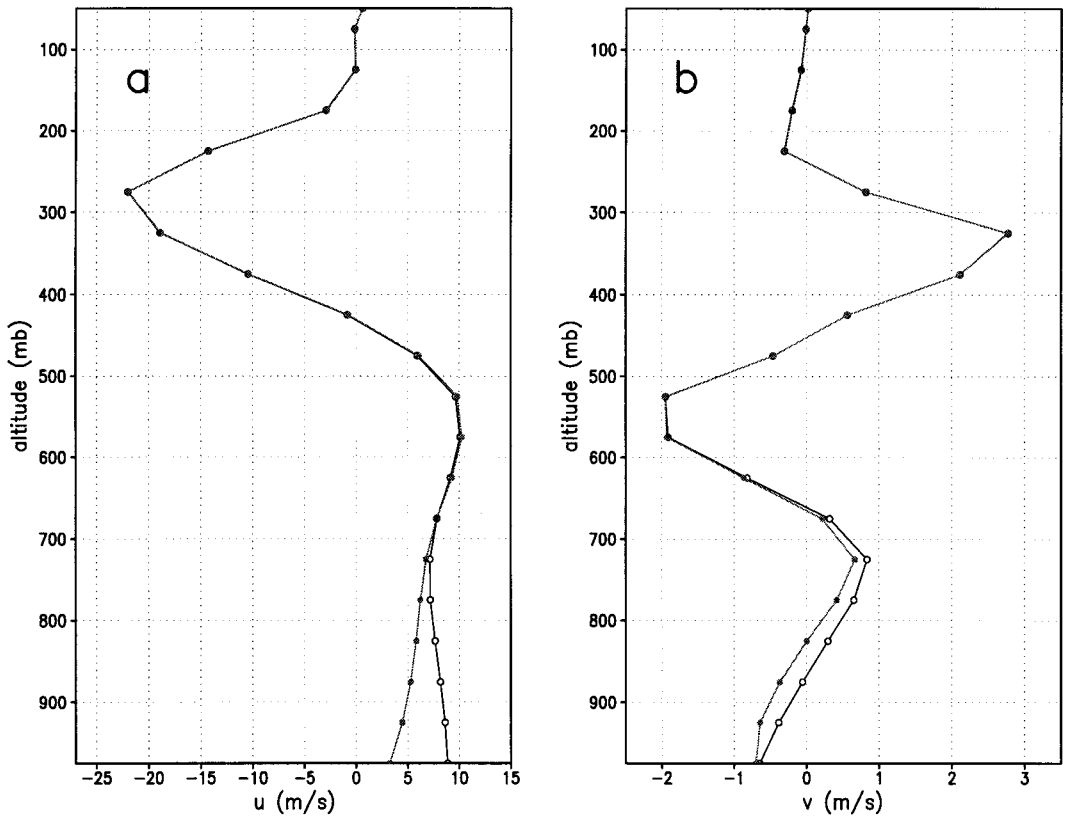

FIG. 13. (a) Vertical profile of zonal wind at 180° longitude and equator for the case with surface momentum flux (solid dots) and with no surface flux (open circles). (b) Same as (a) but for meridional wind at 10.4°N, 230.6°E.

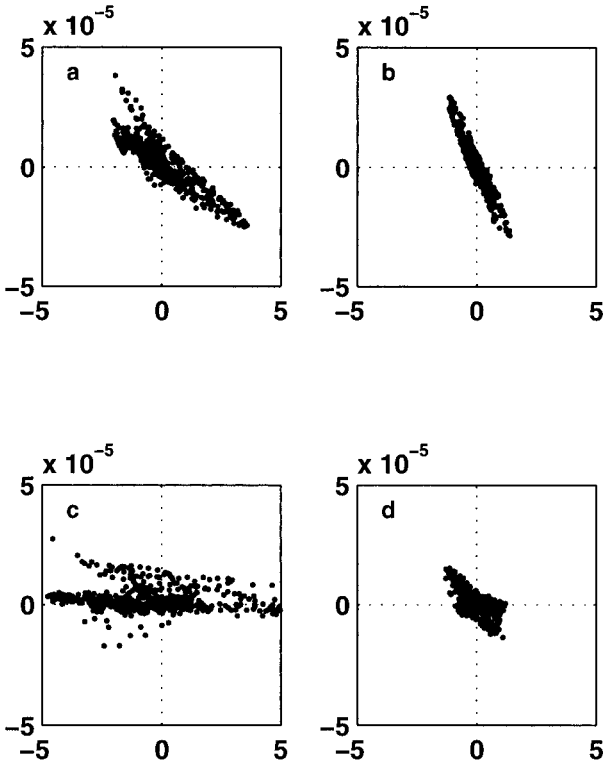

FIG. 14. (a) Scatterplot of the residual zonal momentum geostrophic balance vs zonal wind for the case with surface flux. Points are taken at the 975-mb level globally between 16.36°S and 16.36°N. The negative slope of the best-fit line through these points is the best estimate of the linear u friction coefficient. (b) Same as (a) but for the meridional momentum balance. Note the steeper slope of the points as compared to (a) indicating a larger linear friction coefficient. (c) and (d) As in (a) and (b) but for the no surface momentum flux ($Y = 0$) case.

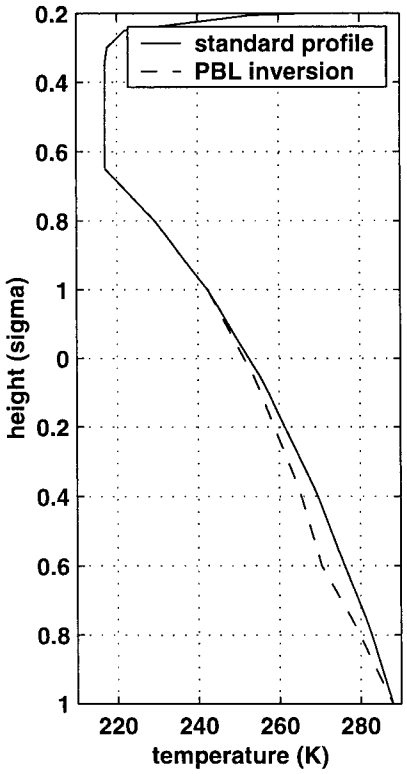

FIG. 15. Basic-state vertical temperature profile used in the model. The solid line represents the standard profile used in the model runs, and the dashed line the modified profile with an inversion at the PBL top height used in the sensitivity study (section 7f).

version strength, whereas the surface heating response *increases* with increasing inversion strength, consistent with our result with both forcings and our interpretation of what each forcing does.

Our result thus suggests that increasing PBL inversion strength reduces the impact of elevated heating on surface flow but increases the impact of surface forcing. It is difficult to test the full implications of this result within our current dynamical framework, as the model vertical resolution is too poor to resolve the PBL inversion adequately. However, our results do support the LN contention that surface forcing is important in regions (primarily the cold tongue regions) where the PBL inversion is strong.

8. Summary and discussion

a. Summary

We study the relative roles of elevated heating and SST gradients in forcing anomalous surface winds over tropical oceans in an idealized GCM with imposed forcing derived from data. Our main conclusion is that, for the two cases of forcing studied with our model, elevated heating dominates the anomalous zonal wind forcing in the Tropics and the meridional wind response in the subtropics. Surface forcing dominates the meridional response in strong SSTA gradient regions near the equator. Since the model fields generally correspond well with observations, we suggest that our conclusions hold for the real atmosphere.

Our model is forced by elevated heating (cumulus convection) and SST gradients—the two thermal contributions thought to most influence surface pressure gradients in the Tropics. We include in our model what we believe are the necessary dynamics and physics to model the influence of these forcings on surface flow: the 3-D linearized primitive equations on a sphere with 20 equispaced sigma levels parameterization of radiation through a simple Newtonian cooling, and the inclusion of an Ekman boundary layer for momentum. Rayleigh friction is applied in the upper and middle atmosphere as a crude proxy for nonlinear processes. Orography is also included in our model. Elevated heating is imposed in the model with an assumed profile, but allowing for a variable peak heating level. The thermal influence of the surface is communicated to the boundary layer by relaxing those levels to the imposed SSTA. Unlike the Gill and Lindzen-Nigam models, we

make no assumptions about the vertical propagation of elevated heating signals to the surface, nor do we assume the absence of any free troposphere influence on surface pressure gradients driven directly by SST.

The observed forcing and surface wind response fields are generated through a multivariate EOF of anomalous monthly precipitation, SST, and 975-mb zonal and meridional winds from January 1979 to December 1998. Two regions are considered: the tropical Pacific region (20°S–20°N, 120°–280°E), and the tropical Atlantic (20°S–20°N, 70°W–20°E). The Pacific EOF 1 pattern is characteristic of the ENSO mature phase, whereas the Atlantic EOF 1 pattern is associated with the tropical Atlantic dipole mode. The above precipitation and SSTA EOF fields force the model, and the output compared with observed 975-mb winds. By employing a suitable cost function for the difference between model and observed fields, we tune the eight model parameters to give the best fit of model to observations. The tuned parameters are within a physically reasonable range, lending confidence to the suitability of this model for surface wind study. The tuning highlights the sensitivity of the surface wind response to the structure of the elevated heating. In particular, the tropical Pacific case favors a heating profile peaking around 400 mb, whereas the tropical Atlantic case favors a profile peaking lower in altitude. In both cases the model produces wind fields resembling the observed, the Pacific case being quite close. We then simply investigate the role of each forcing by imposing them in turn.

We tested the wider applicability of the model by simulating the climatological JJA eddy surface winds and the monthly anomalous surface wind field for January 1979–December 1998. The model, using the parameter settings derived for the tropical Pacific case, performed adequately in both cases. We show that, in contrast to the study of Lindzen and Nigam (1987), that the eddy wind field in the model is driven primarily by elevated heating. We also showed the failure of the model in simulating winds over the west coasts of subtropical northern and southern Africa and the Americas.

We performed sensitivity studies to understand the relative roles of each physical mechanism in the model. Changing the vertical profile of heating strongly affected the 975-mb zonal wind response, and to a lesser extent the meridional response. The response increased with decreasing level of the heating peak. The Ekman boundary layer is crucial in attenuating the wind response near the surface relative to the free atmosphere. It accounts for the observed linear relationship between the residual of the geostrophic balance and the appropriate wind component, including the observed difference between the meridional and zonal linear friction coefficients. Topography has little effect on the flow in the interior of the basin, but has possible significant effect near the coastlines. Increasing the Newtonian cooling rate has little effect on surface flow. Both the thermal PBL height and relaxation rate impacts significantly on the meridional wind component in regions where surface forcing is strong. Finally, increasing the PBL top inversion strength in the basic-state vertical temperature profile significantly decreases the magnitude of the surface flow due to elevated heating, and significantly increases the magnitude of the surface flow due to surface forcing. This final result supports the LN contention that surface forcing is important in regions where the PBL inversion is strong.

b. Why is the model tropical Atlantic simulation poor?

There are two possible reasons why the tropical Atlantic simulation was poor: either the model is lacking the necessary physics or our interpretation of the cause and effect relationship between observed winds and forcings is incorrect.

1) MISSING PHYSICS

We mentioned before the lack of transient eddies in our model; we speculate on four additional contributing causes.

- Lack of land surface heating. Land may have a significant influence on tropical Atlantic surface winds. For example, Li and Philander (1997) show that the seasonal cycle of surface winds in the Gulf of Guinea in the eastern equatorial Atlantic is primarily in response to seasonal variations in land temperatures.
- Changes to the eddy momentum flux due to changes in the barotropic stability of the subtropical jet in the Atlantic (and also the central Pacific) basins. The importance of eddy momentum flux was demonstrated in previous studies comparing two-dimensional axially symmetric and full three-dimensional calculations of the Hadley circulation (e.g., Hess et al. 1993, their Figs. 4a and 15a).
- Inadequate boundary layer parameterization. The marine boundary layer plays a crucial role in determining the surface expression of winds. The discrepancy may be a result of the overly simple Ekman boundary layer parameterization used; in practice, the viscosity and surface drag depends on local conditions. Wallace et al. (1989) demonstrate the effect of surface conditions in the eastern equatorial Pacific in determining the coupling between surface winds and winds above the boundary layer. Chiang and Zebiak (2000) also demonstrate the role of boundary layer height in determining friction at the surface. Furthermore. nonlinear and vertical mixing processes have been shown to play a complex and important role in cross-equatorial PBL flow (e.g., Mahrt 1972a,b; Bond 1992), processes that are not accounted for in our model study. The fit of our model winds to observations may have been lacking precisely because of these missing physics.
- The influence of stratus cloud decks. We noted (cf.

section 6b) the total failure of the model in simulating the month-to-month variability of anomalous winds over the stratus deck regions. Stratus decks may affect surface winds in two ways: indirectly, by affecting SST (Philander et al. 1996); and directly, through diabatic cooling just above the atmospheric boundary layer and heating below it. It is this direct effect that is not represented in our model, and may be a significant forcing on the surface circulation, as proposed and modeled by Nigam (1997). He hypothesized that seasonal cloud radiative forcing due to eastern Pacific stratus decks would drive a southerly surface flow over the eastern Pacific; this flow would increase meridional cold advection and latent heat flux that in turn are conducive for formation of stratocumulus, thus resulting in a feedback mechanism. This hypothesis has been recently supported through analysis of cloud radiative forcing by Bergman and Hendon (2000). Our results are consistent with Nigam's (1997) hypothesis for a greater role of stratus decks in forcing surface winds.

2) CAUSE AND EFFECT IN THE EOF FIELDS

Our modeling procedure assumes that the SST and precipitation fields obtained from the EOF analysis are the cause of the surface winds; however, a reverse situation where the winds force the SST is also possible. This is likely to be the case for the northern tropical Atlantic, where several recent observational and modeling studies (e.g., Chang et al. 1997; Seager et al. 2000; Giannini et al. 2000) have suggested that much of the SST variability there is associated with anomalous surface fluxes from variability of the northeasterly trades, and that variability of the northeasterly trades originate from external influences, in particular ENSO and the North Atlantic Oscillation. This justifies, in hindsight, our choice in optimizing our model over a restricted latitude domain (12°N and S) near the equator, where the link between the applied forcings and winds is more convincing. Our model results support the suggestion that much of the variability of the northeasterly trades originate from outside the tropical Atlantic.

c. Implications for tropical Atlantic variability studies

The relative roles of elevated heating and surface temperature gradients in driving surface winds have implications for the way we conceptualize air–sea interaction. The dominant mode of tropical Atlantic variability accounted for by SST and precipitation combined (excluding the role of land) is associated with a meridional temperature gradient near the equator, and associated cross-equatorial winds (cf. Fig. 2). The winds are viewed as a product of the temperature gradient, in the manner of LN (e.g., Hastenrath and Grieschar 1993; Wagner 1996; Chang et al. 1997). Chang and Philander (1994) postulated an unstable coupled air–sea mode relating the SST dipole with the meridional cross-equatorial winds. Our results suggest that this is in fact the correct zeroth-order picture for both the eastern Pacific and western Atlantic, and that the ITCZ responds largely to this surface circulation caused by the surface temperature gradient.

There is the suggestion (cf. Fig. 4) that in the eastern Pacific, the ITCZ appears to have little impact on the surface circulation there, and so it may appear that boundary layer processes alone are crucial for determining the ITCZ. This interpretation requires some caution, since the applied heating profile may not be entirely correct for that region. This is due to the fact that a single heating profile is applied for the entire tropical Pacific case, and that the optimization may have preferentially chosen a ''higher'' heating profile characteristic of the western and central Pacific, rather than a ''lower'' profile characteristic of eastern Pacific ITCZ heating. We have shown in the sensitivity studies (section 7a) how a lower heating profile increases its surface wind response. The tropical Atlantic case, with its lower heating profile, may give a more realistic assessment on the role of the ITCZ: the Atlantic ITCZ is shown to impact surface wind, in particular the zonal winds in the equatorial region, and both components of winds away from the equator (cf. Fig. 7). The anomalous zonal winds generated by the displaced ITCZ may influence equatorial SST through ocean dynamical processes, and the winds off the equator may feed back positively on the SST there through its effect on surface fluxes.

If these feedbacks turn out to be important, then the paradigm of local generation of tropical Atlantic climate variability must be changed to incorporate the mechanics of the ITCZ. It also introduces the possibility that *external* processes may influence tropical Atlantic surface climate variability, through influencing Atlantic ITCZ behavior; for example, the hypothesized anomalous Walker circulation influence (Saravanan and Chang 2000; Chiang et al. 2000). What drives surface wind over the tropical Atlantic is fundamental to understanding the causes and consequences of tropical Atlantic climate variability.

9. Postscript

A reviewer made us aware of a similar extraction and modeling analysis by Nigam and Chung (2000), with similar conclusions. The results were derived independently of each other, and first submitted for publication at about the same time. The papers differ in the model and reanalysis data used (Nigam and Chung used European Centre for Medium-Range Weather Forecasts reanalysis and Community Climate Model version 3 results) and in regions of diagnosis (both papers investigated ENSO variability, and we additionally examined tropical Atlantic variability).

Acknowledgments. JCHC thanks R. Seager, M. Rozendaal, R. Kleeman, and S. Khatiwala for useful conversations during the course of this work. We are grateful to D. Battisti, Z. Wu, and S. Nigam for extensive comments and suggestions on an earlier version of the paper. A. Giannini provided the topography used in this model. Much of the data gathering and manipulation was done through the web-based IRI/LDEO Climate Data Library developed by B. Blumenthal. This work was supported by NOAA Grant NA67GP0299 (IRI) to SEZ, and NSF Grant ATM99-86515 and NASA Grant JPLCIT 957647 to MAC; JCHC was supported by a NASA Earth Systems Science Fellowship. This is Lamont-Doherty Earth Observatory Contribution Number 6068.

REFERENCES

Battisti, D. S., E. S. Sarachik, and A. C. Hirst, 1999: A consistent model for the large-scale steady surface atmospheric circulation in the Tropics. *J. Climate,* **12,** 2956–2964.

Bergman, J. W., and H. H. Hendon, 2000: The impact of clouds on the seasonal cycle of radiative heating over the Pacific. *J. Atmos. Sci.,* **57,** 545–566.

Bond, N. A., 1992: Observations of planetary boundary-layer structure in the eastern equatorial Pacific. *J. Climate,* **5,** 699–706.

Chang, P., and S. G. H. Philander, 1994: A coupled ocean–atmosphere instability of relevance to the seasonal cycle. *J. Atmos. Sci.,* **51,** 3627–3648.

——, L. Ji, and H. Li, 1997: A decadal climate variation in the tropical Atlantic Ocean from thermodynamic air–sea interactions. *Nature,* **385,** 516–518.

Chiang, J. C. H., and S. E. Zebiak, 2000: Surface wind over tropical oceans: Diagnosis of the momentum balance, and modeling the linear friction coefficient. *J. Climate,* **13,** 1733–1747.

——, Y. Kushnir, and S. E. Zebiak, 2000: Interdecadal changes in eastern Pacific ITCZ variability and its influence on the Atlantic ITCZ. *Geophys. Res. Lett.,* **27,** 3687–3690.

DeMott, C. A., and S. A. Rutledge, 1998: The vertical structure of TOGA COARE convection. Part II: Modulating influences and implications for diabatic heating. *J. Atmos. Sci.,* **55,** 2748–2762.

Deser, C., 1993: Diagnosis of the surface momentum balance over the tropical Pacific Ocean. *J. Climate,* **6,** 64–74.

Geisler, J. E., and D. E. Setevens, 1982: On the vertical structure of damped steady circulation in the Tropics. *Quart. J. Roy. Meteor. Soc.,* **108,** 87–93.

Giannini, A., Y. Kushnir, and M. A. Cane, 2000: Interannual variability of Caribbean rainfall, ENSO and the Atlantic Ocean. *J. Climate,* **13,** 297–311.

Gill, A. E., 1980: Some simple solutions for heat-induced tropical circulation. *Quart. J. Roy. Meteor., Soc.,* **106,** 447–462.

Hartmann, D. L., H. H. Hendon, and R. A. Houze, 1984: Some implications of the mesoscale circulations in tropical cloud clusters for large-scale dynamics and climate. *J. Atmos. Sci.,* **41,** 113–121.

Hastenrath, S., and L. Greischar, 1993: Circulation mechanisms related to northeast Brazil rainfall anomalies. *J. Geophys. Res., Atmos.,* **98** (D3), 5093–5102.

Hess, P. G., D. S. Battisti, and P. J. Rasch, 1993: Maintenance of the intertropical convergence zones and the large-scale tropical circulation on a water-covered Earth. *J. Atmos. Sci.,* **50,** 691–713.

Kalnay, E., and Coauthors, 1996: The NCEP/NCAR 40-Year Reanalysis Project. *Bull. Amer. Meteor. Soc.,* **77,** 437–471.

Kanamitsu, M., 1989: Description of the NMC Global data assimilation and forecast scheme. *Wea. Forecasting,* **4,** 335–342.

Li, T., and B. Wang, 1994: A thermodynamic equilibrium climate model for monthly mean surface winds and precipitation over the tropical Pacific. *J. Atmos. Sci.,* **51,** 1372–1385.

——, and S. G. H. Philander, 1997: On the seasonal cycle of the equatorial Atlantic Ocean. *J. Climate,* **10,** 813–817.

Lindzen, R. S., and S. Nigam, 1987: On the role of sea surface temperature gradients in forcing low level winds and convergence in the Tropics. *J. Atmos. Sci.,* **44,** 2418–2436.

——, E. S. Batten, and J.-W. Kim, 1968: Oscillations in atmospheres with tops. *Mon. Wea. Rev.,* **96,** 133–140.

Mahrt, L. J., 1972a: A numerical study of the influence of advective accelerations in an idealized, low-latitude, planetary boundary layer. *J. Atmos. Sci.,* **29,** 1477–1484.

——, 1972b: A numerical study of the coupling between the boundary layer and free atmosphere in an accelerated low-latitude flow. *J. Atmos. Sci.,* **29,** 1485–1495.

Murphree, T., and H. van den Dool, 1988: Calculating winds from time mean sea level pressure fields. *J. Atmos. Sci.,* **45,** 3269–3281.

Neelin, J. D., 1989: On the interpretation of the Gill model. *J. Atmos. Sci.,* **46,** 2466–2468.

Nelder, J. A., and R. Mead, 1965: A simplex method for function minimization. *Comput. J.,* **7,** 308–313.

Nigam, S., 1997: The annual warm to cold phase transition in the eastern equatorial Pacific: Diagnosis of the role of stratus cloud-top cooling. *J. Climate,* **10,** 2447–2467.

——, and H.-S. Shen, 1993: Structure of oceanic and atmospheric low-frequency variability over the tropical Pacific and Indian Oceans. Part I: COADS observations. *J. Climate,* **6,** 657–676.

——, and C. Chung, 2000: ENSO surface winds in CCM3 simulation: Diagnosis of errors. *J. Climate,* **13,** 3172–3186.

Philander, S. G. H., D. Gu, D. Halpern, G. Lambert, N. C. Lau, T. Li, and R. C. Pacanowski, 1996: Why the ITCZ is mostly north of the equator. *J. Climate,* **9,** 2958–2972.

Rossow, W. B., A. W. Walker, D. E. Beuschel, and M. D. Roiter, 1996: International satellite cloud climatology project (ISCCP) documentation of new cloud datasets. WMO/TD-No.737, WMO, 55 pp.

Saravanan, R., and P. Chang, 2000: Interaction between tropical Atlantic variability and El Niño–Southern Oscillation. *J. Climate,* **13,** 2177–2194.

Sardeshmukh, P. D., and B. Hoskins, 1985: Vorticity balances in the Tropics during the 1982–83 El Niño–Southern Oscillation event. *Quart. J. Roy. Meteor. Soc.,* **111,** 261–278.

Seager, R., and S. E. Zebiak, 1995: Simulation of tropical climate with a linear primitive equation model. *J. Climate,* **8,** 2497–2520.

——, Y. Kushnir, M. Visbeck, N. Naik, J. Miller, G. Krahmann, and H. Cullen, 2000: Causes of Atlantic Ocean climate variability between 1958 and 1998. *J. Climate,* **13,** 2845–2862.

Thompson, R. M., S. W. Payne, E. E. Recker, and R. J. Reed, 1979: Structure and properties of synoptic-scale wave disturbances in the Intertropical Convergence Zone of the eastern Atlantic. *J. Atmos. Sci.,* **36,** 53–72.

Wagner, R. G., 1996: Mechanisms controlling variability of the interhemispheric sea surface temperature gradient in the tropical Atlantic. *J. Climate,* **9,** 2010–2019.

——, and A. M. Da Silva, 1994: Surface conditions associated with anomalous rainfall in the Guinea coastal region. *Int. J. Climatol.,* **14,** 179–199.

Wallace, J. M., T. P. Mitchell, and C. Deser, 1989: The influence of sea surface temperature on surface wind in the eastern equatorial Pacific: Seasonal and interannual variability. *J. Climate,* **2,** 1492–1499.

Wang, B., and T. Li, 1993: A simple tropical atmosphere model of relevance to short-term climate variations. *J. Atmos. Sci.,* **50,** 260–284.

Wu, Z. H., E. S. Sarachik, and D. S. Battisti, 1998: Thermally forced surface winds on an equatorial beta-plane. *J. Atmos. Sci.,* **56,** 2029–2037.

——, D. S. Battisti, and E. S. Sarachik, 1999a: Rayleigh friction,

Newtonian cooling, and the linear response to steady tropical heating. *J. Atmos. Sci.,* **57,** 1937–1957.

——, E. S. Sarachik, and D. S. Battisti, 1999b. Vertical structure of convective heating and the three-dimensional structure of the forced circulation in the Tropics. *J. Atmos. Sci.,* **57,** 2169–2187.

Xie, P., and P. A. Arkin, 1997: Global precipitation: A 17-year monthly analysis based on gauge observations, satellite estimates, and numerical model outputs. *Bull. Amer. Meteor. Soc.,* **78,** 2539–2558.

Xie, S.-P., 1999: A dynamic ocean–atmosphere model of the tropical Atlantic climate variability. *J. Climate,* **12,** 64–70.

——, and G. H. Philander, 1994: A coupled ocean–atmosphere model of relevance to the ITCZ in the eastern Pacific. *Tellus,* **46A,** 340–350.

Zebiak, S. E., 1982: A simple atmospheric model of relevance to El Niño. *J. Atmos. Sci.,* **39,** 2017–2027.

——, 1986: Atmospheric convergence feedback in a simple model for El Niño. *Mon. Wea. Rev.,* **114,** 1263–1271.